**Universidade de Aveiro** Departamento de Física,
2010

**José Daniel Lago da Silva Neves Gouveia**

# The helicoidal Hubbard model

# O modelo de Hubbard helicoidal

**Universidade de Aveiro** Departamento de Física,
**2010**

**José Daniel Lago da Silva Neves Gouveia**

# The helicoidal Hubbard model

Dissertation presented in University of Aveiro for the fulfilling of the requirements for obtaining the master's degree in Physics, advised by R. G. Dias, Professor in the Department of Physics of the University of Aveiro

## the jury

| | |
|---|---|
| presidente / president | **Armando Neves**<br>Professor Associado da Universidade de Aveiro (por delegação da Reitora da Universidade de Aveiro) |
| vogais / examiners committee | **Ricardo G. Dias**<br>Professor Auxiliar da Universidade de Aveiro (orientador) |
| | **Miguel António da Nova Araújo**<br>Professor Auxiliar da Universidade de Évora |

**acknowledgements**

It is with great pleasure that I use this opportunity to thank everyone who helped me during the writing of this thesis.

Firstly, and most important of all, my advisor, Professor Ricardo Dias, for the strong motivation, patience and understanding, the constant availability and of course, the most accurate scientific advice I received.

Secondly, to those few selected who, without knowing it, made this a more pleasant task. My brother Sdjz, for his help with some mathematical details, Pedro Silva, for showing me a different string theory, my mother Margarida, for always insisting I return home before dawn, Dina Prazeres, for her displays of inflexible determination and granting me invaluable laughter and fun even when all the work seems lost, Paulo Santos, Elisabete Capelo and Diogo Baptista, for keeping me company while doping silicon, geostrophic winds, and $TiO_2$, respectively, and finding one of the best places to eat francesinhas, Alexandre Lopes, for teaching me how the food vending machine works, Nara Angelo, for the convincing examples of conviction at work, Álvaro Almeida and JCM "Pico" for the teachings on LateX programming and troubleshooting, and Joana Rodrigues for often inviting me for events which do not involve presentations, numerical calculations, or headaches because the peak on the density of states or the spectral function is not where it should be.

Lastly, it is adequate to thank every person I know who did not bother me while I was working.

## Abstract

The Hubbard model is one of the most simple models to describe the motion and interaction of electrons in solids. It has been widely studied due to its applications in the description of organic conductors and in the search for high $T_c$ superconductivity.

In this work, the Hubbard model in a helicoidal lattice is studied, a lattice identical to the two-dimensional square lattice in the thermodynamic limit. The magnetic phases of this model are analyzed by building mean field phase diagrams. The thermodynamics of this model is studied in the strong coupling limit ($U \to \infty$). We consider hoppings along and across helix steps. The hoppings across helix steps generate a mixing of the spin configurations, whose dynamics is also studied.

## Resumo

O modelo de Hubbard é um dos modelos mais simples para descrever o movimento e a interacção de electrões em sólidos. Tem sido largamente estudado pelas suas aplicações na descrição de condutores orgânicos e na procura de supercondutividade a cada vez mais altas temperaturas.

Neste trabalho, é estudado o modelo de Hubbard numa rede helicoidal, uma rede idêntica à rede bidimensional quadrada no limite termodinâmico. As fases magnéticas deste modelo são analisadas através da construção de diagramas de fase em campo médio. A termodinâmica deste modelo é estudada no limite de acoplamento forte ($U \to \infty$). São considerados saltos ao longo de passos da hélice e saltos de um passo para outro. Os saltos entre diferentes passos da hélice geram mistura das configurações de spin, cuja dinâmica também é estudada.

# Contents

**1 Introduction** **1**

**2 The helicoidal tight-binding model** **5**
- 2.1 "Square" lattices . . . . . 5
- 2.2 Helicoidal lattice . . . . . 5
  - 2.2.1 General case . . . . . 6
  - 2.2.2 Tight-binding case ($U = 0$) . . . . . 6

**3 Mean field phase diagram of the Hubbard model** **11**
- 3.1 One dimension . . . . . 12
  - 3.1.1 Ferromagnetism . . . . . 12
  - 3.1.2 Antiferromagnetism . . . . . 14
- 3.2 General case . . . . . 15
- 3.3 Helix . . . . . 19

**4 The Hubbard model in the strong coupling limit ($U/t \to \infty$)** **23**
- 4.1 The $t_\perp = 0$ limit with one hole . . . . . 23
- 4.2 The $t_\perp = 0$ limit with $N_h$ holes . . . . . 25
- 4.3 Counting the $q$ states . . . . . 27
  - 4.3.1 Mielke's approach . . . . . 27
  - 4.3.2 A simpler approach . . . . . 27
  - 4.3.3 Results . . . . . 30
- 4.4 Thermodynamics . . . . . 34

**5 The quantum spin queue model** **39**
- 5.1 The $t_\perp \neq 0$ limit with one hole and one up spin . . . . . 39
  - 5.1.1 The $\Delta$-permutation operator . . . . . 39
  - 5.1.2 The effect of $t_\perp$ in the spin configurations . . . . . 40
  - 5.1.3 The hole hopping term . . . . . 41
  - 5.1.4 The spin exchange term . . . . . 41
- 5.2 The $t_\perp \neq 0$ limit with $N_h$ holes . . . . . 42
  - 5.2.1 The $N_h = 1$ case . . . . . 44

**6 Spectral function** **47**
- 6.1 1D Hubbard model . . . . . 47
- 6.2 Helicoidal Hubbard model . . . . . 48

**7 Conclusions** **51**

**A Correlation functions for spinless fermions** **53**

**B The Möbius inversion formula** **55**

## Chapter 1

# Introduction

One of the most important problems in theoretical solid state physics is the Hubbard model. This model describes electronic correlations in narrow energy bands. In one dimension (1D), it describes the dynamics of organic conductors, while its twodimensional (2D) version can be applied to high temperature superconductivity [1] (see Fig. 1.1). Hans Bethe [3] found the exact solution of the 1D Hubbard Model (wave functions of Bethe ansatz), while the solution for higher dimensions is still not known [4].

The Hubbard model was independently introduced by John Hubbard, Gutzwiller and Kanamori [5] around the same time. The Hubbard Hamiltonian has only two parameters: a hopping amplitude $t$, describing the motion of electrons in the lattice, and an interaction amplitude $U$, which describes the interaction between electrons. The general form of the Hubbard Hamiltonian assumes the Born-Oppenheimer approximation, i.e., considers a solid consisting of nuclei forming a static lattice and electrons which can hop between the atoms of the lattice. For the cases considered in this work, we will also consider the tight-binding approximation, only allowing electrons to hop between nearest neighbor atoms and only on-site interaction between electrons.

Under these assumptions, the Hubbard Hamiltonian is

$$H = -t \sum_{\langle l,l' \rangle} c^{\dagger}_{l,\sigma} c_{l',\sigma} + U \sum_{l} n_{l\uparrow} n_{l\downarrow}, \tag{1.1}$$

where $\langle l, l' \rangle$ denotes nearest neighbor pairs of sites, $c^{\dagger}_{l,\sigma}$ and $c_{l,\sigma}$ are the fermion creation and annihilation operators on site $l$ with spin $\sigma$ and $n_{l,\sigma}$ is the respective particle number operator. The effect of the Hamiltonian is show in Fig. 1.2.

In this work, three types of lattice will be studied (Fig. 1.3):

- 1D lattice with periodic boundary conditions, equivalent to a ring;
- 2D lattice with periodic boundary conditions, equivalent to a torus;
- helicoidal lattice, similar to the 2D lattice, but with twisted boundary conditions.

Depending on the number of dimensions, hopping may be allowed along various directions. In the case of a helix, electrons can hop along a helix pitch, and across nearest pitches as well (Fig. 1.4). The tight-binding limit ($U = 0$) includes no interaction term and the strong coupling limit ($U \to \infty$) does not allow double occupancies. The 1D Hubbard model in the strong coupling limit has an algebraic solution [6] [7].

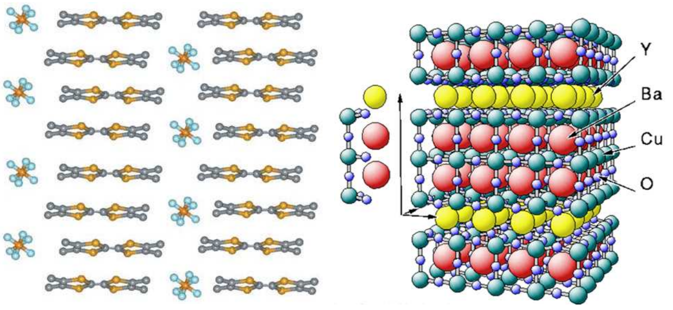

Figure 1.1: The one-dimension Hubbard model describes the dynamics of organic conductors. On the left, several molecules of TMTCF, a salt intensively explored and the model system of quasi one-dimensional conductors is shown [2]. Its two-dimensional version is applied to high-temperature superconductivity. The Yttrium barium copper oxide (YBCO) is shown on the right, a high temperature superconductor).

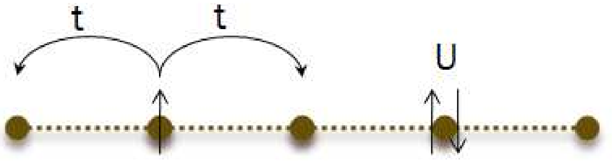

Figure 1.2: The tight-binding approximation and on-site interaction between electrons.

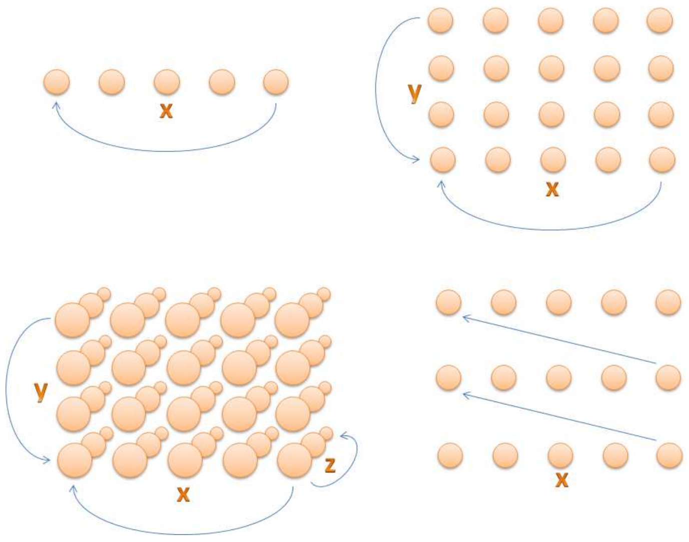

Figure 1.3: The types of lattice considered in this work: 1D ring (top left), 2D torus (top right), 3D with periodic boundaries (bottom left, only presented for reference) and helicoidal (bottom right).

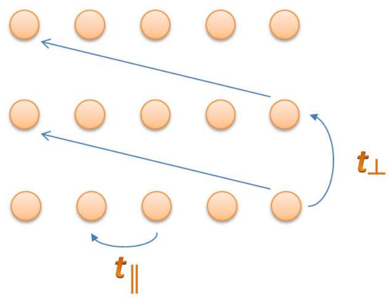

Figure 1.4: Illustrating the effects of $t_\parallel$ and $t_\perp$ upon the electrons.

Several approximations have been made in order to obtain solutions for the 2D Hubbard model, like the 1+1 dimensional Hubbard model using wave functions of Bethe ansatz [8] and a helical Hubbard model in which first-neighbor and third-neighbor hoppings are included [9].

In this work, the helicoidal Hubbard model is presented as one quite similar to the 2D one (square lattice). The main difference is that the helix involves *twisted boundary contitions*, that is, when an electron (or a hole) reaches the end of a row, by hopping in the same direction successively, it then hops to a neighbor row in the helix model, while it hops to the other end of the row where it was in the 2D model.

Some of the advantages of studying the helicoidal model instead of the 2D one are that the degeneracy of the tight-binding approximation for the helix with $t_\perp = 0$ is much lower than the same approximation for the 2D model with $t_y = 0$, and the eigenstates of the helicoidal model with $t_\perp = 0$ remain eigenstates when $t_\perp$ becomes finite. Another advantage is the 1D labeling of sites and the consequent unidimensional wave number of the particles.

The crucial approximation in the study of the helicoidal Hubbard model is the assumption that the atoms (sites) in a helix pitch are much closer to each other than sites on different helix pitches. Consequently, we will be working in the limit

$$U \gg t_\parallel \gg t_\perp \gg \frac{t_\parallel^2}{U}, \tag{1.2}$$

where, as shown in Fig. 1.4, $t_\parallel$ and $t_\perp$ denote the hopping terms between atoms in the same helix section, and in adjacent helix pitches, respectively.

## Organization of the thesis

In chapter 2, the solution of the tight-binding ($U = 0$) helicoidal model is presented and compared to the 1D and 2D tight-binding models.

In chapter 3, using the mean field approximation, *filling versus interaction parameter* phase diagrams are built for the 1D, 2D and helicoidal Hubbard models, emphasizing ferro- and antiferromagnetism in these models. Ferromagnetic, antiferromagnetic and spiral phases are addressed.

In chapter 4, the helicoidal Hubbard model is solved exactly for $t_\perp = 0$ (Hubbard chain) and in the strong coupling limit ($U \to \infty$), for any number $N_h$ of holes. Thermodynamic functions of this model are studied.

In chapter 5, the quantum spin queue model is introduced, as a tool to tackle the problem of $t_\perp \neq 0$; we solve the model with only one hole and one inverted spin to study the effect of $t_\perp$

on the spin configuration and the motion of holes (thus factorizing the $t_\perp$ term), and finally solve the more general case with $N_h$ holes.
In chapter 6, using some of the results from the previous chapter, the spectral function associated to the helicoidal Hubbard model is numerically calculated.
Finally, a short summary of the conclusions of all chapters is presented.

## Chapter 2

# The helicoidal tight-binding model

In this chapter, we simplify the Hubbard Hamiltonian by considering only the tight-binding term, and neglecting the interaction term. It becomes very easy to solve under any of the geometries of this work. The solutions for "square" lattices are presented, as well as the helicoidal lattice, which is defined in this chapter as well.

### 2.1 "Square" lattices

The solution of the Hubbard model considering only the tight-binding term, i. e., setting $U = 0$, is known and quite simple. In a D-dimensional square lattice, the solution is

$$E = -2 \sum_{d=1}^{D} t_d \cos k_d, \tag{2.1}$$

where $d$ labels the dimensions $(x_1, \cdots, x_d)$ and

$$k_d = \frac{2\pi}{L_d} n_d \qquad n_d = 0, 1, ..., L_d - 1, \tag{2.2}$$

$L_d$ being the number of sites in the $d$ direction.

### 2.2 Helicoidal lattice

A helix is a space curve with parametric equations

$$\begin{array}{l} x = r\ \cos(t) \\ y = r\ \sin(t) \\ z = c\ t \end{array} \ , \tag{2.3}$$

where $r$ is the radius of the helix and $2\pi c$ is the vertical pitch between the helix's loops.

The helicoidal model is a special case of a 2-dimensional Hubbard model, since we naturally generate all possible positions of a particle using only one parameter, for example:

$$\begin{pmatrix} 10 & 11 & 12 \\ 7 & 8 & 9 \\ 4 & 5 & 6 \\ 1 & 2 & 3 \end{pmatrix}. \tag{2.4}$$

If this situation was of cylindrical geometry, such as a torus, it would be equivalent to four 3-site Hubbard rings (plus allowing hopping between corresponding sites in the first and last rings), and mixing in the spin configurations would take place due to hoppings both at the boundaries of the cylinder, at those of each row, and between corresponding sites of adjacent rings. In a helicoidal lattice, however, spin configurations are only mixed when the particle/hole hops from site 12 to 1, or vice versa, and between corresponding sites in different helix pitches.

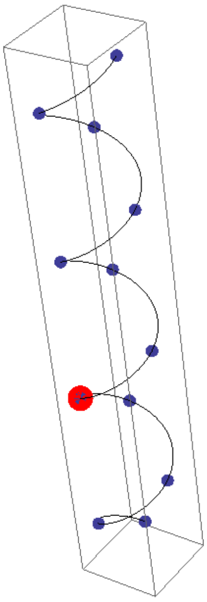

Figure 2.1: Representation of a helix with 12 sites ($L = 12$), 4 loops of arc length 3 ($\Delta = 3$) along it and a hole on site 5.

---

### 2.2.1 General case

For the helix, we will consider the Hamiltonian

$$H = -t_{\parallel} \sum_{j,\sigma} (c^{\dagger}_{j+1,\sigma} c_{j,\sigma} + c^{\dagger}_{j,\sigma} c_{j+1,\sigma}) - t_{\perp} \sum_{j,\sigma} (c^{\dagger}_{j+\Delta,\sigma} c_{j,\sigma} + c^{\dagger}_{j,\sigma} c_{j+\Delta,\sigma}) + U \sum_{j} n_{j,\uparrow} n_{j,\downarrow}, \quad (2.5)$$

where

- $j$ labels all sites on the helix as a 1D system;
- $t_{\parallel}$ is the value of the overlap integral between nearest neighbors along the helix (equivalent to $t_{j,j+1}$ in a 1D lattice);
- $t_{\perp}$ is the value of the overlap integral between nearest neighbors across the helix (equivalent to $t_{j,j+\Delta}$ in a 1D lattice, see figure 2.1);
- $c^{\dagger}_{j,\sigma}$ and $c_{j,\sigma}$ are again the creation and destruction operators of a fermion with spin $\sigma$ on site $j$, respectively.

We will work in the limit $U \gg t_{\parallel} \gg t_{\perp} \gg t^2_{\parallel}/U$. The reason to consider $t_{\parallel} \gg t_{\perp}$ is that the distance between sites is in principle smaller for adjacent ones (along the helix) than for sites in different helix steps, resulting in a larger orbital overlap along a helix step than across it.

### 2.2.2 Tight-binding case ($U = 0$)

For $U = 0$, the helicoidal model becomes very similar to the 2D tight-binding model, as mentioned above. Its energy dispersion relation is

$$E_k = -2t_{\parallel} \cos(k) - 2t_{\perp} \cos(k\Delta), \quad (2.6)$$

with $k = 2\pi n/L$ and $n = 0, 1, ..., L-1$. Assuming $\Delta$ is an integer (and therefore $\Delta$ is the number of sites $L$ divided by the number of helix steps), as $t_\perp$ increases from 0 to values of the same order of $t_\perp$, the solution approaches that of the 2D model in the thermodynamic limit. This can be shown by representing the density of states of both models (Fig. 2.2).

In expression 2.6, only one momentum variable, $k$, was used to describe a behavior that is equivalent to the 2D tight-binding one in the thermodynamic limit:

$$E_{k_x,k_y} = -2t_{\|}\cos(k_x) - 2t_\perp\cos(k_y), \tag{2.7}$$

with

$$\begin{array}{ll} k_x = \frac{2\pi}{L_x}n_x & n_x = 0, \cdots, L_x - 1 \\ k_y = \frac{2\pi}{L_y}n_y & n_y = 0, \cdots, L_y - 1. \end{array} \tag{2.8}$$

Imposing a twisted boundary condition upon the 2D model along the $x$ direction so that the phase gained by hopping $L_x$ sites along the $x$ direction is the same as hopping one site along the $y$ direction (Fig. 2.3):

$$e^{ik_xL_x} = e^{ik_y}. \tag{2.9}$$

This condition is equivalent to

$$\begin{array}{ll} k_x = \frac{2\pi}{L_x}n_x & = \frac{k_y}{L_x} + \frac{2\pi}{L_x}n' \\ & = \frac{k_y}{Lx} + k'_x. \end{array} \tag{2.10}$$

The equivalence between the two models requires $L_x = \Delta$ and $L_y = L/\Delta$. We can therefore write the dispersion relation for the 2D model with twisted boundary conditions

$$E'_{k_x,k_y} = -2t_{\|}\cos\left(\frac{k_y}{\Delta} + k'_x\right) - 2t_\perp\cos(k_y), \tag{2.11}$$

and, comparing 2.11 and 2.6 ($\Delta = L_x$),

$$k = \frac{k_y}{\Delta} + k'_x \Leftrightarrow k\Delta = k_y + 2\pi n', \tag{2.12}$$

or, in terms of $n$,

$$\frac{2\pi n\Delta}{L} = \frac{2\pi n_y}{L/\Delta} + 2\pi n' \Leftrightarrow n = n_y + \frac{L}{\Delta}n', \tag{2.13}$$

and consequently,

$$\begin{array}{l} n' = \mathrm{int}\left(\frac{n}{L/\Delta}\right) \\ n_y = \mathrm{mod}\left(n, \frac{L}{\Delta}\right). \end{array} \tag{2.14}$$

From equation 2.11, two relations between $k$ and $(k'_x, k_y)$ can be obtained, but they are equivalent, meaning that 2.12 is enough for the helicoidal and 2D models to be equivalent in the thermodynamic limit. These expressions will be used in the following chapters for comparing the 2D model with the helicoidal one.

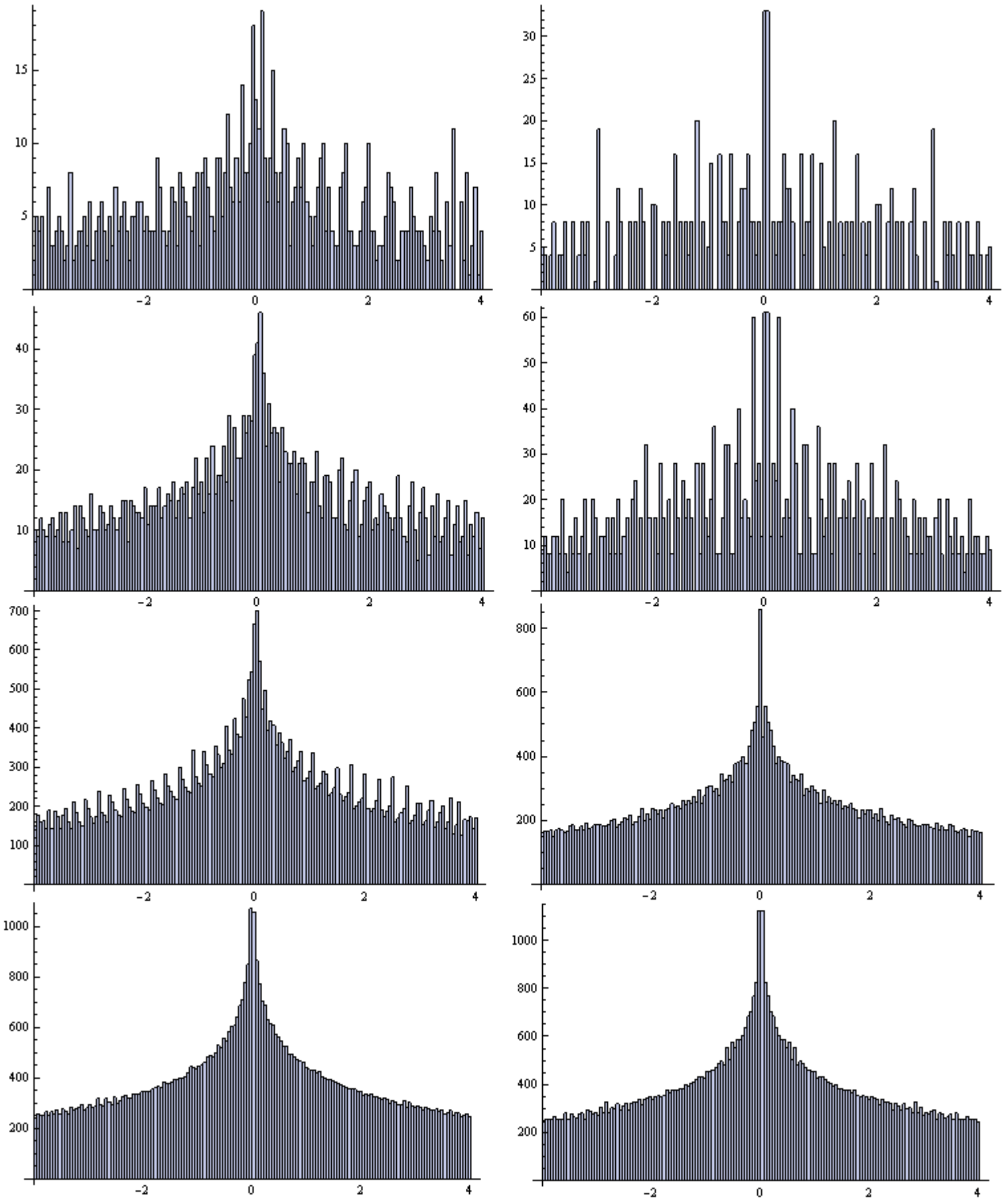

Figure 2.2: Representation of the density of states on a helix (left) and on a torus (right) in the tight-binding limit, considering the lattice constant $a = 1$ and the overlap integrals $t = t_{\perp} = t_{\parallel} = 1$. The number of sites in each case is $900, 2500, 40000, 62500$, from top to bottom. For the torus, $L_x = L_y = 30, 50, 200, 250$ and for the helix, $\Delta = 30, 50, 200, 250$, so that the only difference between the two geometries is the angle mentioned in this section. This fact makes both situations identical as one approaches the thermodynamic limit.

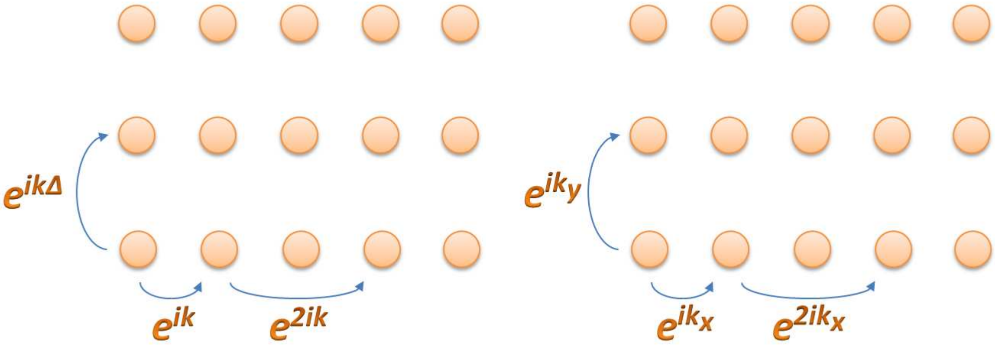

Figure 2.3: A hop along the $x$-direction induces a phase $e^{ik}$ on a helix (left) or $e^{ik_x}$ on a 2D lattice (right). A hop along the $y$-direction induces a phase $e^{ik\Delta}$ on a helix or $e^{ik_y}$ on a bidimensional model. On a helix, hopping $\Delta = L_x$ times in the $x$-direction induces a phase $e^{ik\Delta} = e^{ik_x\Delta} = e^{ik_xL_x} = e^{ik_y}$, when a twisted boundary condition is imposed upon the 2D model.

## Chapter 3

# Mean field phase diagram of the Hubbard model

The objective of this thesis is to consider both the tight-binding and interaction terms. In the previous chapter, the energy dispersion relation for the tight-binding term was presented. In this chapter, we consider the full Hamiltonian and use the simple mean field approximation to obtain the phase diagrams for the 1D, 2D and helicoidal Hubbard models.

When Hubbard inserted the interaction term into the tight-binding Hamiltonian, the diagonalization of the model became more complicated. The interaction occurs between every electron pair in the system, but the diagonal terms (on-site repulsion) are about one order of magnitude greater than the other repulsion terms. Considering only on-site interaction, the Hamiltonian can be written as

$$H = -t \sum_{\langle l,l' \rangle,\sigma} \left( c^{\dagger}_{l,\sigma} c_{l',\sigma} + c^{\dagger}_{l',\sigma} c_{l,\sigma} \right) + U \sum_{l} c^{\dagger}_{l,\uparrow} c_{l,\uparrow} c^{\dagger}_{l,\downarrow} c_{l,\downarrow}, \tag{3.1}$$

where $\langle l, l' \rangle$ denotes any nearest neighbor pair of sites.

The difficulty lies upon the interaction term because it is quartic in the fermionic operators. The mean field approach reduces the quartic dependence to a more simple quadratic one, using the mean values of the particle number operators $n_{l,\sigma} = c^{\dagger}_{l,\sigma} c_{l,\sigma}$. Depending on how those mean values are chosen, one will find different types of magnetism in the Hubbard model [10]:

- in a paramagnetic configuration, the density of spins $n_{l,\sigma}$ is the same for all sites $l$ and spins $\sigma$;
- in a ferromagnetic configuration, the density of spins depends on the spin $\sigma$ but not on $l$;
- in an antiferromagnetic configuration, $n_{l,\sigma}$ varies with both site and spin;
- in a spiral state, we assume magnetic moments are aligned in the $x - y$ plane according to $\vec{S}_{\vec{j}} = \frac{m}{2} \left( \cos(\vec{Q} \cdot \vec{j}), \sin(\vec{Q} \cdot \vec{j}) \right)$, where $\vec{Q}$ determines the alignment of spins in each direction and $\vec{j} = (j_x, j_y)$ is the position of the site. In 1D, both $\vec{Q}$ and $\vec{j}$ are numbers. For example, $Q = 0$ along a certain direction generates ferromagnetic states along that direction, and $Q = \pi$ gives antiferromagnetic ones.

In this chapter, mean field theory will be used to generate phase diagrams for one- and two-dimensional "square" lattices, as well as the helicoidal model. Note that phase transitions only occur in three dimensions, but mean field theory predicts phase transitions for any number of dimensions. The results presented in this chapter for 1D and 2D are, however, relevant to weakly coupled 1D or 2D systems so that they actually become 3D and phase transitions may occur.

## 3.1 One dimension

Let us first address the 1D case and build the phase diagrams for its ferromagnetic and antiferromagnetic configurations.

### 3.1.1 Ferromagnetism

Under mean field, we write

$$n_{l,\sigma} = n_\sigma + (n_{l,\sigma} - n_\sigma), \tag{3.2}$$

thus considering the average value of $n$ is the same on every site, but it varies with the spin $\sigma$ (ferromagnetism). In the Hamiltonian, the particle number operators appear as $n_{l,\uparrow}n_{l,\downarrow}$ (quartic in the fermionic operators), which becomes

$$\begin{aligned} n_{l,\uparrow}n_{l,\downarrow} &= (n_\uparrow + (n_{l,\uparrow} - n_\uparrow))\,(n_\downarrow + (n_{l,\downarrow} - n_\downarrow)) \\ &\approx n_\uparrow n_\downarrow + n_\uparrow(n_{l,\downarrow} - n_\downarrow) + (n_{l,\uparrow - n_\uparrow})n_\downarrow \\ &= n_\uparrow n_{l,\downarrow} + n_{l,\uparrow}n_\downarrow - n_\uparrow n_\downarrow. \end{aligned} \tag{3.3}$$

Here, $n_\uparrow$ and $n_\downarrow$ represent the average density of ↑ and ↓ spins, respectively (that is, the average number of each spin, per site).

The diagonal form of the first term in the Hamiltonian 3.1 is known:

$$-2t\sum_{k,\sigma}\cos k \;\; c^\dagger_{k,\sigma}c_{k,\sigma}, \tag{3.4}$$

for one dimension, considering only nearest neighbor hopping. If $L$ is the number of sites, $k$ can take $L$ values:

$$k = \frac{2\pi}{L}(-L/2 + n_k) \qquad n_k = 1, 2, ..., L, \tag{3.5}$$

for $L$ even.

Because of the mean field approach and since we are considering a ferromagnetic system, the interaction term immediately becomes diagonal, and the eigenvalues of the full Hamiltonian are

$$E = E_\uparrow(k_\uparrow) + E_\downarrow(k_\downarrow) - Un_\uparrow n_\downarrow, \tag{3.6}$$

where

$$\begin{aligned} E_\uparrow &= -2t\cos k_\uparrow + Un_\downarrow \\ E_\downarrow &= -2t\cos k_\downarrow + Un_\uparrow. \end{aligned} \tag{3.7}$$

The possible values of $k$ are the same for both spins, up and down.

For each total number of particles $N$ ($N_\uparrow$ spin up particles plus $N_\downarrow$ spin down particles), the value of $U$ determines whether the ground state is paramagnetic or ferromagnetic. Let us define a magnetization $m$ such that

$$m = \frac{n_\uparrow - n_\downarrow}{n_\uparrow + n_\downarrow}, \tag{3.8}$$

where, again,

$$\begin{aligned} n_\uparrow &= N_\uparrow/N \\ n_\downarrow &= N_\downarrow/N. \end{aligned} \tag{3.9}$$

We can represent the energy of the system as a function of the magnetization (see, for example, Fig. 3.1). The ground state will be paramagnetic if the minimum energy occurs for

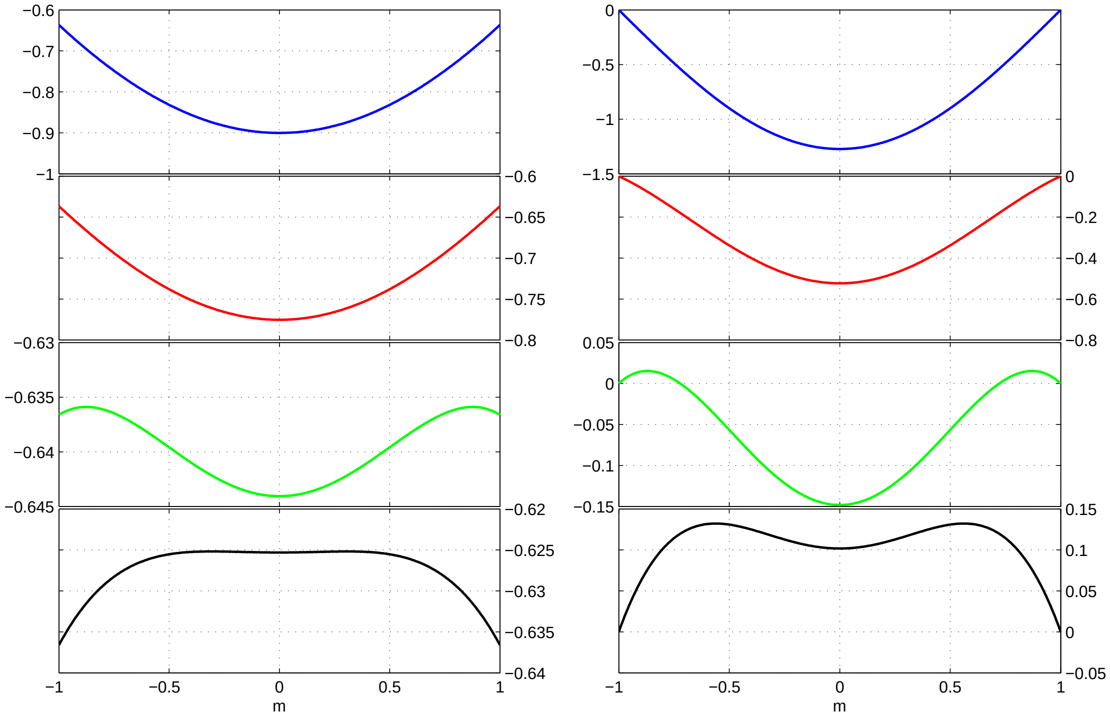

Figure 3.1: Representation of the energy per site $E/L$ as a function of the magnetization $m$ for $U = 0$, $U = 2$, $U = 4.1$ and $U = 4.4$ (from top to bottom) for the 1D ferromagnetic Hubbard model at quarter (half) filling on the left (right) with $L = 512$, $N = 256$ ($N = 512$) and $t = 1$.

---

$m = 0$ and ferromagnetic otherwise. Computationally, this is done fixing the size of the lattice $L$, the number or particles $N$ and the interaction parameter $U$. Then the program loops over the number of up spins from 0 to $N$, adds up the lowest $N_\uparrow$ and the lowest $N_\downarrow$ energy levels, obtaining the total energy $E$, and finally represents how $E$ varies with its respective $m$.

### Quarter filling ($\mathbf{n = 1/2}$)

Quarter filling means we have 1/4 as many particles as the maximum allowed by the $L$ sites ($2L$ particles), so we have $L/2$ particles. Figure 3.1 (left) shows the energy per site, as a function of the magnetization $m$. For very low $U$, the ground state of the system is paramagnetic, because the ground state occurs for $m = 0$. As $U$ increases, the state becomes ferromagnetic. We conclude that, for quarter filling, the phase transition occurs for some value of $U$ between 4.1 and 4.4.

### Half filling ($\mathbf{n = 1}$)

For the half filling case, figure 3.1 (right) shows the energy as a function of the magnetization. Similarly to what happens for quarter filling, a high enough $U$ turns the paramagnetic system into a ferromagnetic one. However, comparing the graphics shows that at half filling the phase transition occurs for a larger $U$.

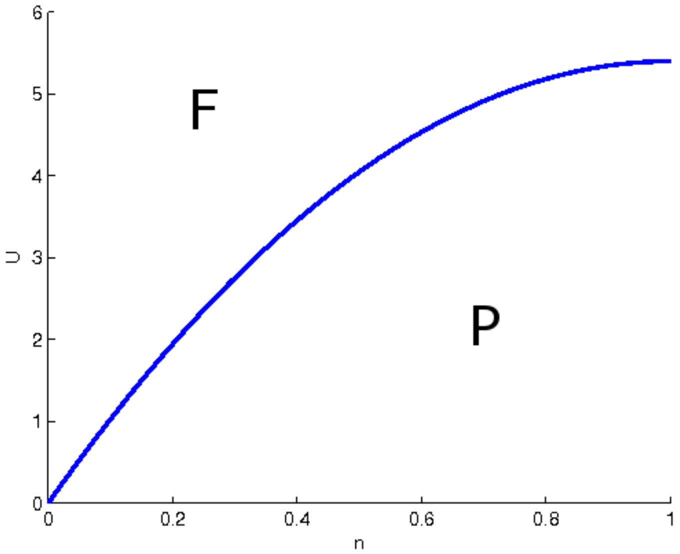

Figure 3.2: Phase diagram for the 1D ferromagnetic Hubbard model with $t = 1$. The horizontal axis contains the filling $n$ (number of particles per site) and the vertical one has the interaction parameter normalized to $t$, $U/t$.

#### Phase diagram

As we have seen, for each different doping of the system, the value of the on-site interaction $U$ that induces the phase transition changes. If one represents, the transition value of $U$ as a function of the doping, one obtains the phase diagram. The phase diagram shows us if the behavior of the system is paramagnetic or ferromagnetic for each pair $(n, U)$. Figure 3.2 shows the phase diagram of the Hubbard model described using our mean field approach for ferromagnetism.

### 3.1.2 Antiferromagnetism

As mentioned above, in a ferromagnetic configuration, the density of spins ↑ and ↓ is independent of the site, that is, $n_{l,\uparrow} = n_\uparrow$, $n_{l,\downarrow} = n_\downarrow$, while in an antiferromagnetic configuration, all sites alternate between a higher density of up or down spins:

$$n_{l,\uparrow} = n + (-1)^l m, \qquad n_{l,\downarrow} = n - (-1)^l m, \tag{3.10}$$

meaning even sites have an extra density of up spins and odd sites have an extra density of down spins.

Since the average density of spin depends upon the parity of the site, the Hamiltonian for the 1D antiferromagnetic Hubbard model can be written as

$$H = -t \sum_{j,\sigma} \left( c^\dagger_{j,\sigma} c_{j+1,\sigma} + c^\dagger_{j+1,\sigma} c_{j,\sigma} \right) + U \sum_{j \text{ even}} \left( n_{j,\uparrow} n_{j,\downarrow} + n_{j+1,\uparrow} n_{j+1,\downarrow} \right), \tag{3.11}$$

where $j$ even represents all even sites. Unlike the case of ferromagnetism, the diagonalization of this Hamiltonian does not follow trivially after applying mean field theory. Using equation

3.10, the interaction term becomes

$$U\sum_j \left[\left(n+(-1)^j m\right) n_{j,\downarrow} + \left(n-(-1)^j m\right) n_{j,\uparrow} - (n+m)(n-m)\right]. \tag{3.12}$$

Applying the Fourier transforms of the creation and annihilation operators and further replacing $(-1)^j$ by $e^{i\pi j}$ gives

$$\begin{aligned} H &= \sum_k \left(-2t\cos k c^\dagger_{k,\uparrow} c_{k,\uparrow} + Unc^\dagger_{k,\uparrow} c_{k,\uparrow} - Umc^\dagger_{k+\pi,\uparrow} c_{k,\uparrow}\right) + \\ &+ \sum_k \left(-2t\cos k c^\dagger_{k,\downarrow} c_{k,\downarrow} + Unc^\dagger_{k,\downarrow} c_{k,\downarrow} + Umc^\dagger_{k+\pi,\downarrow} c_{k,\downarrow}\right) + \\ &- UL(n^2-m^2), \end{aligned} \tag{3.13}$$

where $k$ has the same $L$ values as before, still from $-\pi$ to $\pi$. This Hamiltonian becomes easy to diagonalize for up and down spins separately, after a simple transformation. In fact, one can compute the summation defining $k$ in a reduced zone (from $-\pi/2$ to $\pi/2$) and adding a few terms so that the result remains unchanged. For up spins (the first line in equation 3.13), the matrix

$$H_\uparrow = \begin{pmatrix} -2t\cos k + Un & -Um \\ -Um & 2t\cos k + Un \end{pmatrix} \tag{3.14}$$

follows, assuming the $\{c_{k,\uparrow}, c_{k+\pi,\uparrow}\}$ basis. For down spins, in the $\{c_{k,\downarrow}, c_{k+\pi,\downarrow}\}$ basis, the matrix is

$$H_\downarrow = \begin{pmatrix} -2t\cos k + Un & Um \\ Um & 2t\cos k + Un \end{pmatrix}. \tag{3.15}$$

Despite the fact that the matrices are different, their eigenvalues are the same, i. e., the energy levels for both up and down spins are

$$E_\uparrow(k) = E_\downarrow(k) = \frac{U}{2}(n^2-m^2) + mU \pm \sqrt{(2t\cos k)^2 + (nU)^2} \tag{3.16}$$

where the already diagonal term $UL(n^2-m^2)$ was divided evenly between the two spin types. One must keep in mind that, when compared with the ferromagnetic case, we have only half as many possible values for $k$ ($L/2$, because of the redefinition in the reduced zone), but we also have two different energies for each of them, meaning we still have $L$ energy levels for each spin type.

Computationally, one no longer loops over $N_\uparrow$, but rather over $m = 1/N, 2/N, ..., N/(2L)$. A few plots of the on-site energy as a function of $m$ are shown in figure 3.3. The phase diagram is obtained by finding, for each doping value $n$, the value of $U$ above which the ground state does not occur for $m = 0$. The result is shown in figure 3.4.

## 3.2 General case

For the 2D and helicoidal cases, we shall use a more general but similar approach [11] [12] to that of the 1D case. To make calculations simpler, they will be made for the 1D Hamiltonian, and then generalized to the 2D case. We begin by applying Fourier transforms to the fermion creation and annihilation operators in Hamiltonian 3.1,

$$c_{j\sigma} \to \frac{1}{\sqrt{L}} \sum_k e^{ikj} a_{k\sigma} \tag{3.17}$$

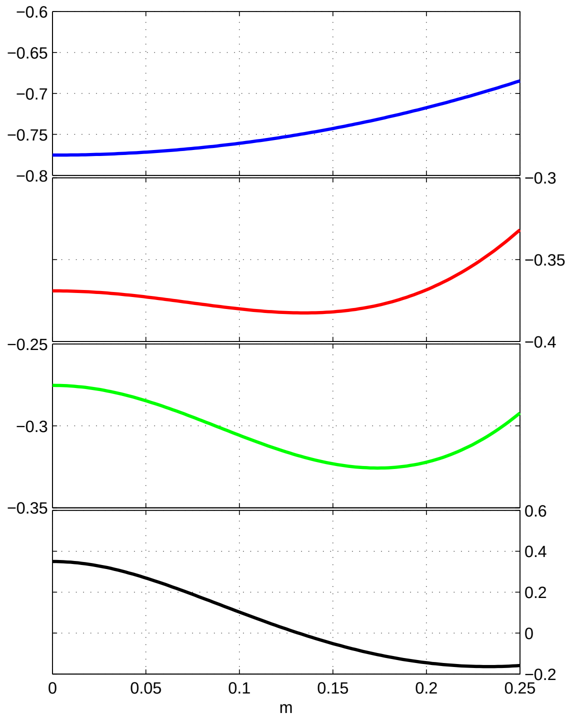

Figure 3.3: Plot of the energy per site $E/L$ as a function of the staggered magnetization $m$ for $U = 2$, $U = 8.5$, $U = 10$ and $U = 20$ (from top to bottom) for the 1D antiferromagnetic Hubbard model at quarter filling with $L = 256$, $N = 128$ and $t = 1$.

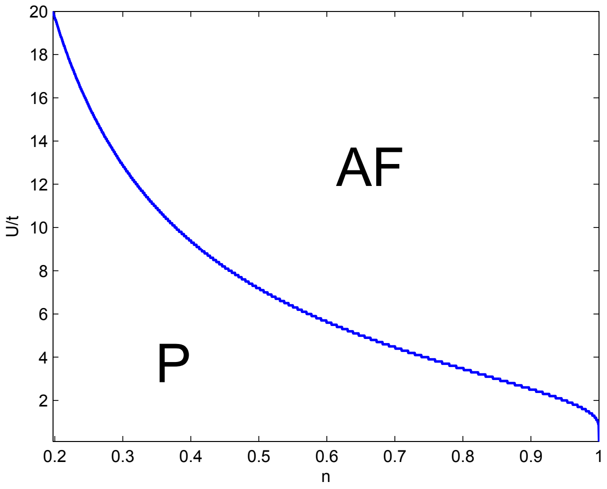

Figure 3.4: Representation of the phase diagram for the 1D antiferromagnetic Hubbard model. The horizontal axis contains the filling $n$ (number of particles per site) and the vertical one has the interaction parameter normalized to $t$, $U/t$.

$$c^\dagger_{j\sigma} \to \frac{1}{\sqrt{L}} \sum_{k'} e^{-ik'j} a^\dagger_{k'\sigma}. \tag{3.18}$$

We then obtain, for the tight-binding term of the Hamiltonian,

$$\begin{aligned} H_t &= -t \sum_j c^\dagger_{j\uparrow} c_{j+1\uparrow} + c^\dagger_{j+1\uparrow} c_{j\uparrow} + c^\dagger_{j\downarrow} c_{j+1\downarrow} + c^\dagger_{j+1\downarrow} c_{j\downarrow} \\ &= -2t \sum_k (a^\dagger_{k\uparrow} a_{k\uparrow} + a^\dagger_{k\downarrow} a_{k\downarrow}) \cos k, \end{aligned} \tag{3.19}$$

where a diagonal form was obtained using no mean field approximations, because, as mentioned before, mean field will only be necessary to transform the quartic $U$-term in the Hamiltonian into a more simple quadratic one. Applying Fourier transforms to the interaction term of the Hamiltonian gives,

$$\begin{aligned} H_U &= U \sum_j c^\dagger_{j\uparrow} c_{j\uparrow} c^\dagger_{j\downarrow} c_{j\downarrow} \\ &= \tfrac{U}{L^2} \sum_j \sum_{k_1} \sum_{k_2} \sum_{k_3} \sum_{k_4} e^{-i(k_1-k_2+k_3-k_4)j} a^\dagger_{k_1\uparrow} a_{k_2\uparrow} a^\dagger_{k_3 j} a_{k_4\downarrow}. \end{aligned} \tag{3.20}$$

From the summation over $j$, one concludes,

$$\begin{aligned} & k_1 - k_2 + k_3 - k_4 = 0 \\ & \quad \Rightarrow k_3 - k_2 = k_4 - k_1 = Q \\ & \quad \Rightarrow \begin{cases} k_3 = k_2 + Q \\ k_4 = k_1 + Q \end{cases} \end{aligned}, \tag{3.21}$$

where $Q = 2\pi n/L$, with $n = 0, \cdots, L-1$, because it is the difference between two values of $k$. Denoting $k_1 = k$ and $k_2 = k'$, the expression simplifies to

$$H_U = \sum_{k,k'} a^\dagger_{k\uparrow} a_{k'\uparrow} a^\dagger_{k'+Q\downarrow} a_{k+Q\downarrow} \tag{3.22}$$

Now that we have the interaction term expressed in $k$-space, the application of mean field yields the result

$$\begin{aligned} H_{U,MF} = U \sum_{k,k'} (&\langle a^\dagger_{k\uparrow} a_{k'\uparrow} \rangle a^\dagger_{k'+Q\downarrow} a_{k+Q\downarrow} \\ &+ \langle a^\dagger_{k'+Q\downarrow} a_{k+Q\downarrow} \rangle a^\dagger_{k\uparrow} a_{k'\uparrow} \\ &- \langle a^\dagger_{k\uparrow} a_{k'\uparrow} \rangle \langle a^\dagger_{k'+Q\downarrow} a_{k+Q\downarrow} \rangle \\ &- \langle a^\dagger_{k\uparrow} a_{k+Q\downarrow} \rangle a^\dagger_{k'+Q\downarrow} a_{k'\uparrow} \\ &- \langle a^\dagger_{k'+Q\downarrow} a_{k'\uparrow} \rangle a^\dagger_{k\uparrow} a_{k+Q\downarrow} \\ &+ \langle a^\dagger_{k\uparrow} a_{k+Q\downarrow} \rangle \langle a^\dagger_{k'+Q\downarrow} a_{k'\uparrow} \rangle) \end{aligned} \tag{3.23}$$

We shall consider the magnetic moments are aligned on the $x-y$ plane. Therefore the $z$-component of the local spin operator

$$\vec{S}_j = \sum_{\alpha,\alpha'=\uparrow,\downarrow} c^\dagger_{j,\alpha} \vec{\sigma}_{\alpha\alpha'} c_{j,\alpha'}, \tag{3.24}$$

where $\vec{\sigma} = (\sigma_x, \sigma_y, \sigma_z)$ is the Pauli vector, we conclude that the averages that couple spins in the same direction are zero on every site (as that coupling is made using the $\sigma_z$ matrix).

Replacing [12] $\langle a^\dagger_{k+Q\downarrow} a_{k\uparrow}\rangle = -\Delta_Q/U$, where $\Delta_Q$ is the gap parameter, we obtain

$$H_{U,MF} = \sum_k \Delta_Q a^\dagger_{k+Q\downarrow} a_{k\uparrow} + \Delta_Q a^\dagger_{k\uparrow} a_{k+Q\downarrow} + \frac{\Delta_Q^2}{U}. \tag{3.25}$$

Joining the results $H_t$ and $H_{U,MF}$, we obtain the final expression for the Hamiltonian,

$$\begin{aligned} H_{MF} \quad = \quad & \sum_k \left(-2t\cos k + \frac{\Delta_Q^2}{U}\right) a^\dagger_{k\uparrow} a_{k\uparrow} + \left(-2t\cos(k+Q) + \frac{\Delta_Q^2}{U}\right) a^\dagger_{k+Q\downarrow} a_{k+Q\downarrow} \\ & + \Delta_Q a^\dagger_{k+Q\downarrow} a_{k\uparrow} + \Delta_Q a^\dagger_{k\uparrow} a_{k+Q\downarrow}, \end{aligned} \tag{3.26}$$

or, in matrix form,

$$H_{MF} = \sum_k \begin{pmatrix} \epsilon_k + \frac{\Delta_Q^2}{U} & \Delta_Q \\ \Delta_Q & \epsilon_{k+Q} + \frac{\Delta_Q^2}{U} \end{pmatrix}, \tag{3.27}$$

where $\epsilon_k = -2t\cos k$ is the part of the Hamiltonian that changes when we change the dimensionality or geometry of the system. The eigenvalues are

$$E_{MF} = \sum_k \left[\frac{1}{2}\left(\epsilon_k + \epsilon_{k+Q} \pm \sqrt{(\epsilon_k - \epsilon_{k+Q})^2 + 4\Delta_Q^2}\right) + \frac{\Delta_Q^2}{U}\right] \tag{3.28}$$

The $x$- and $y$- components of the spin operator $\vec{S}_j$ are, for real $\Delta_Q$,

$$S^x_j = \frac{\Delta_Q}{U}\cos(Q\cdot j), \tag{3.29}$$

$$S^y_j = \frac{\Delta_Q}{U}\sin(Q\cdot j). \tag{3.30}$$

Defining the order parameter $m_Q = 2\Delta_Q/U$, we obtain the expectation values of $S^\pm_j$,

$$S^\pm_j = \frac{1}{2} m_Q e^{\pm iQ\cdot j}. \tag{3.31}$$

Generalizing these results to the bidimensional model, the eigenvalues of the Hamiltonian are the same, but

$$\epsilon_k = -2t(\cos k_x + \cos k_y), \tag{3.32}$$

and

$$S^\pm_{\vec{j}} = \frac{1}{2} m_Q e^{\pm i\vec{Q}\cdot\vec{j}} = \frac{1}{2} m_Q e^{\pm i(Q_x j_x + Q_y j_y)}. \tag{3.33}$$

One easily realizes that changing $\vec{Q}$ changes the relative alignment of the spins. For example, $Q = 0$ on a certain direction implies ferromagnetism along that direction, and $Q = \pi$ generates antiferromagnetism. $\vec{Q} = (0, \pi)$ leads to ferromagnetism along the $x$ direction, and antiferromagnetism along $y$. Fig. 3.5 shows the spin configurations for a few values of $Q$ in an arbitrary direction. We obtain a phase diagram for each $\vec{Q}$. For the specific values $\vec{Q} = (0,0)$ and $\vec{Q} = (\pi,\pi)$, the eigenvalues simplify, respectively, to

$$E_F = \sum_k \left[\frac{\Delta_Q^2}{U} + \frac{1}{2}\left(2\epsilon_k \pm 2\Delta_Q\right)\right] = \sum_k \left[\frac{\Delta_Q^2}{U} - 2t(\cos k_x + \cos k_y) \pm \Delta_Q\right] \tag{3.34}$$

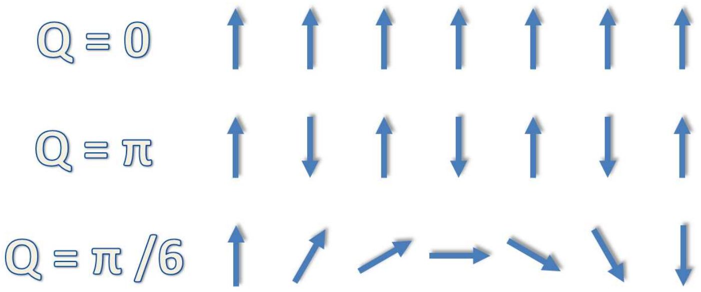

Figure 3.5: Spin configurations for some values of $Q$ in an arbitrary direction.

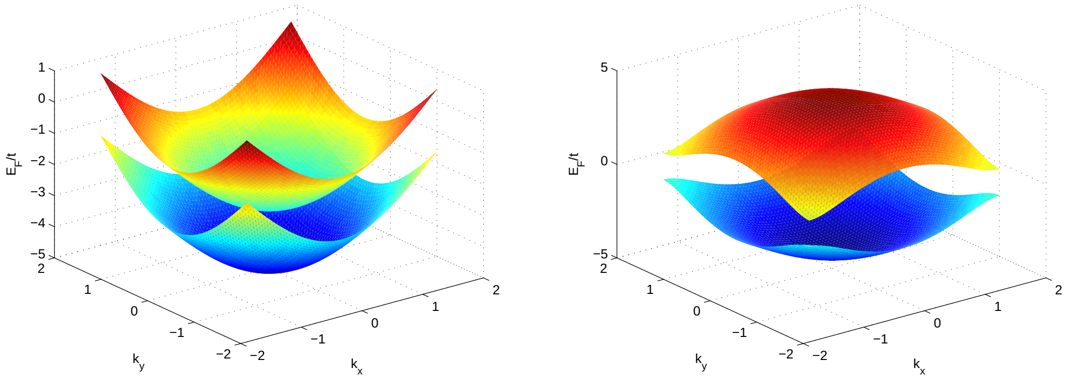

Figure 3.6: Dispersion relations obtained using the approach in [11] for the 2D Hubbard model, considering $mU = 2$, and $\vec{Q} = (0,0)$ (the ferromagnetic limit, left) and $\vec{Q} = (\pi,\pi)$ (the antiferromagnetic limit, right)

$$E_{AF} = \sum_k \left[ \frac{\Delta_Q^2}{U} \pm \frac{1}{2}\sqrt{4\epsilon_k^2 + 4\Delta_Q^2} \right] = \sum_k \left[ \frac{\Delta_Q^2}{U} \pm \sqrt{4t^2(\cos k_x + \cos k_y)^2 + \Delta_Q^2} \right]. \qquad (3.35)$$

These two dispersion relations are plotted in Fig. 3.6 for $mU = 2$. Fig. 3.7 shows the phase diagram obtained for the 2D Hubbard model for a lattice with 20 × 20 sites. The prediction of a spiral phase for low filling is in agreement with reference [13].

## 3.3 Helix

For the helicoidal Hubbard model, we change $\epsilon_k$ to

$$\epsilon_k = -2t_{\parallel}\cos(k) - 2t_{\perp}\cos(k\Delta), \qquad (3.36)$$

which gives the new eigenvalues when inserted into 3.28. Using these eigenvalues we obtain the phase diagrams for the strong-coupling helicoidal Hubbard model (Fig. 3.8). This Figure shows how the phase diagram of this model evolves, as we move from the 1D case ($t_\perp = 0$) to the helicoidal case with $t_\perp = t_\parallel$.

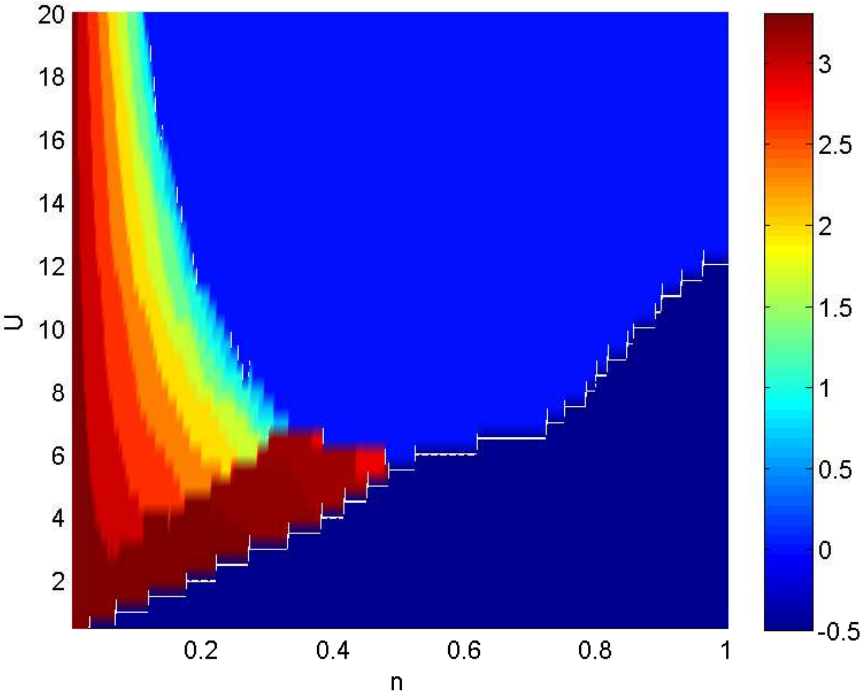

Figure 3.7: Phase diagram for the 20 × 20 2D Hubbard model. Colors represent (positive) values of $Q$ which minimize the energy for each pair $(n, U)$. The "negative" area represents the paramagnetic phase (not negative values of $Q$). The dark blue-colored area (the area around $(n = 0.8, U = 4)$, for example) represents the paramagnetic phase, the light blue area (as in (n=0.5,U=16)) corresponds to the ferromagnetic phase $(\vec{Q} = (0, 0))$ and the darkest red area is the antiferromagnetic phase $(\vec{Q} = (\pi, \pi))$. Although it may seem otherwise, the antiferromagnetic state $(\vec{Q} = (\pi, \pi))$ only occurs very close to the vertical axis $(n = 0)$.

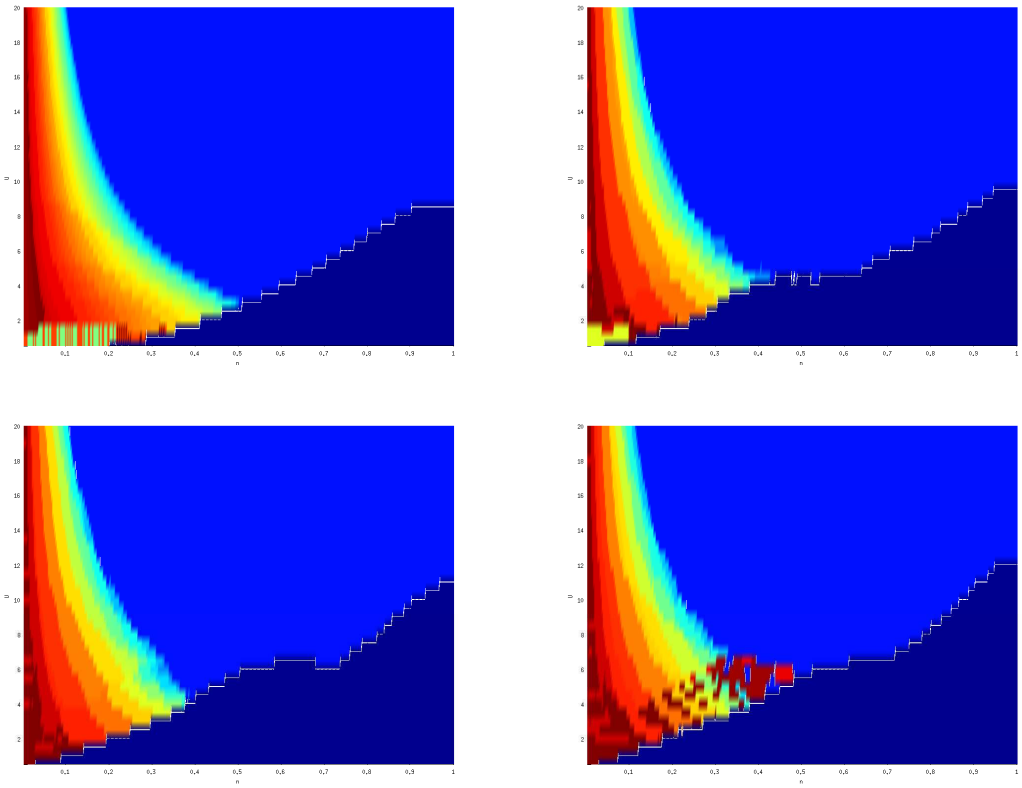

Figure 3.8: Phase diagram for the $20 \times 20$ helicoidal Hubbard model with $t_\perp = 0$ (top left), $t_\perp = 0.5$ (top right), $t_\perp = 0.8$ (bottom left) and $t_\perp = 1$ (bottom right). Colors represent (positive) values of $Q$ which minimize the energy for each pair $(n, U)$. The "negative" area represents the paramagnetic phase (not negative values of $Q$). The area with $Q = 0$ (as in (n=0.5,U=16)) corresponds to the ferromagnetic phase and the dark red area with $Q = \pi$ is the antiferromagnetic phase. Although it may seem otherwise, the antiferromagnetic state ($\vec{Q} = (\pi, \pi)$) only occurs very close to the vertical axis ($n = 0$).

---

Comparing these results with those in [11], we see the states $(Q, \pi)$ and $(0, \pi)$ are strongly modified, meaning there is a strong dependance on these phases upon the boundary conditions. Apart from the $20 \times 20$ lattice, the $30 \times 30$ lattice was also considered, and the results were identical to the ones presented here. Future work will´consist of considering even larger clusters to ensure finite size effects are not greatly affecting our approach.

## Chapter 4

# The Hubbard model in the strong coupling limit ($U/t \to \infty$)

In this chapter, we consider $U \to \infty$, so that all states with double occupancies are pushed to infinite energy and are therefore not allowed. The helicoidal model in the strong coupling limit with $t_\perp = 0$ (equivalent to the $U \to \infty$ Hubbard chain) is solved exactly and some of its thermodynamic properties are studied. In the strong coupling limit, there can only be one or zero particles on each site. This means that the only hoppings allowed are the ones involving holes.

### 4.1 The $t_\perp = 0$ limit with one hole

The helicoidal Hubbard model with $L$ sites, in this limit, is equivalent to a ring with $L$ sites and $N = L - 1$ spins. The possible states can, therefore, be labeled by indicating the position of the hole and the spin configuration on the rest of the ring [7]. For example, the notation

$$|2, \{\sigma_1, \sigma_2, \sigma_3\}\rangle \,, \tag{4.1}$$

represents the state in which the hole is at site 2, and sites 1, 3 and 4 are occupied by spins $\sigma_1$, $\sigma_2$ and $\sigma_3$, respectively (implying the helix has 4 sites). Making the substitution $c_j^\dagger = n_j c_j^\dagger + (1 - n_j) c_j^\dagger$ and dropping the terms associated to double occupancies, the Hamiltonian for such a system is

$$H = -t_\parallel \sum_{j,\sigma} (1 - n_{j,\bar\sigma}) c_{j,\sigma}^\dagger c_{j+1,\sigma} (1 - n_{j+1,\bar\sigma}) + (1 - n_{j+1,\bar\sigma}) c_{j+1,\sigma}^\dagger c_{j,\sigma} (1 - n_{j,\bar\sigma}). \tag{4.2}$$

Considering the hoppings of the particles is equivalent to considering those of the hole. The hoppings of the hole can be described using a simple tight-binding Hamiltonian, but one cannot ignore the spin configuration, because it changes when the hole hops from site $L$ to 1 and vice versa, becoming one of its circular permutations. Let us introduce the circular permutation operator $Q$, such that

$$Q \, |j, \{\sigma_1, \sigma_2, ..., \sigma_{L-1}\}\rangle = |j, \{\sigma_{L-1}, \sigma_1, ..., \sigma_{L-2}\}\rangle \,, \tag{4.3}$$

i. e., the effect of $Q$ on a state $|j, \{\sigma\}\rangle$ is equivalent to causing the hole to perform a full loop around the ring ( = along the helix). The eigenstates of $Q$ are states invariant in a circular permutation:

$$|j, \{\sigma\}, q\rangle = \frac{1}{\sqrt{r_\alpha}} \sum_{m=0}^{r_\alpha - 1} e^{iqm} Q^m \, |j, \{\sigma\}\rangle \,, \tag{4.4}$$

where

- $r_\alpha$ is the periodicity of the spin configuration, that is, the number of times the hole has to perform a full loop around the ring in order for the spins to return to their original configuration;
- $\alpha$ is the label of each set of spin configurations that are circular permutations of each other. Spin configurations with different $\alpha$ cannot be obtained from each other through a circular permutation;
- $q$ is the momentum of the spin configuration

  $$q = \frac{2\pi}{r_\alpha} n, \tag{4.5}$$

  where $n = 0, 1, ..., r_\alpha - 1$.

Applying $Q$ to one of its eigenstates gives

$$\begin{aligned} Q\,|j, \{\sigma\}, q\rangle &= \tfrac{1}{\sqrt{r_\alpha}} e^{-iq} \sum_{m=0}^{r_\alpha - 1} e^{iq(m+1)} Q^{m+1}\,|j, \{\sigma\}\rangle \\ &= e^{-iq}\,|j, \{\sigma\}, q\rangle\,. \end{aligned} \tag{4.6}$$

In order to express the Hamiltonian in this basis, we need to apply $H$ to all its vectors:

- $|j, \{\sigma\}, q\rangle$, with $j = 2, 3, ..., L-1$

  $$H\,|j, \{\sigma\}, q\rangle = t_\parallel\,(|j-1, \{\sigma\}, q\rangle + |j+1, \{\sigma\}, q\rangle) \tag{4.7}$$

- $|1, \{\sigma\}, q\rangle$

  $$\begin{aligned} H\,|1, \{\sigma\}, q\rangle &= t_\parallel\,(|2, \{\sigma\}, q\rangle + Q\,|L, \{\sigma\}, q\rangle) \\ &= t_\parallel\left(|2, \{\sigma\}, q\rangle + e^{-iq}\,|L, \{\sigma\}, q\rangle\right) \end{aligned} \tag{4.8}$$

- $|L, \{\sigma\}, q\rangle$

  $$\begin{aligned} H\,|L, \{\sigma\}, q\rangle &= t_\parallel\left(|L-1, \{\sigma\}, q\rangle + Q^{-1}\,|1, \{\sigma\}, q\rangle\right) \\ &= t_\parallel\left(|L-1, \{\sigma\}, q\rangle + e^{iq}\,|1, \{\sigma\}, q\rangle\right). \end{aligned} \tag{4.9}$$

Note that neither the spin configuration nor its momentum changed after applying the Hamiltonian, so we will drop them from this point. The Hamiltonian in this subspace becomes

$$H = t_\parallel \left[ (|2\rangle + e^{-iq}\,|L\rangle)\,\langle 1| + (|L-1\rangle + e^{iq}\,|1\rangle)\,\langle L| + \sum_{j=2}^{L-1} (|j-1\rangle + |j+1\rangle)\,\langle j| \right]. \tag{4.10}$$

The Hamiltonian can now be made translationally invariant by distributing the phase gain (or loss) among all $L$ sites, instead of being applied only upon the sites at the frontier, thus becoming

$$H = t_\parallel \sum_{j=1}^{L} \left( e^{-iq/L}\,|j\rangle\,\langle j+1| + e^{iq/L}\,|j+1\rangle\,\langle j| \right). \tag{4.11}$$

This Hamiltonian is equivalent to the usual tight-binding model with an external flux $\phi = \phi_0 q/(2\pi) = \phi_0 n/r_\alpha$ (here, $\phi_0 = h/e$ is the flux quantum), whose eigenvectors are

$$|k\rangle = \frac{1}{\sqrt{L}} \sum_{j=1}^{L} e^{ikj} |j\rangle \tag{4.12}$$

with the corresponding eigenvalues

$$E(k) = 2t_\parallel \cos\left(k - \frac{q}{L}\right). \tag{4.13}$$

## 4.2 The $t_\perp = 0$ limit with $N_h$ holes

Because there is now more than one hole, the states will be labeled using a set $\{h\} = \{h_1, \cdots, h_{N_h}\}$ of the positions of the holes and a set $\{\sigma\} = \{\sigma_1, \cdots, \sigma_N\}$ of the positions of the spins:

$$|\{h\}; \{\sigma\}\rangle = \prod_{j=1}^{N} c^\dagger_{b_j,\sigma_j} |0\rangle, \tag{4.14}$$

where $b_j = j + n_j(\{h\})$ and $n_j(\{h\})$ is the number of holes to the left of site $j$.

Let us introduce the slave-fermion representation of the fermionic operators [7] in the zero double occupancy subspace:

- $S^\dagger_{j,\sigma_j}$, the bosonic creation operator of a spin $\sigma_j$ on site $j$;
- $e^\dagger_k$, the fermionic creation operator of a hole on site $k$,

such that $(1 - n_{j,\bar{\sigma}})c^\dagger_{j,\sigma} = S^\dagger_{j,\sigma} e_j$. Using slave-fermion notation, state 4.14 is represented as

$$|\{h\}, \{\sigma\}\rangle = (-1)^{\sum\limits_{j=1}^{N}(b_j - 1)} \prod_{j=1}^{N} S^\dagger_{b_j,\sigma_j} \prod_{k=1}^{N_h} e^\dagger_{h_k} |0\rangle_{sh}, \tag{4.15}$$

where $|0\rangle_{sh}$ is the vacuum for both spins and holes. The first factor is due to the number of times the operator $e_j$ needs to exchange with the $e^\dagger_{h_k}$ operators present in state $\prod\limits_{k=1}^{N_h} e^\dagger_{h_k} |0\rangle_{sh}$. The Hamiltonian (Eq. 4.2) is represented as

$$H = t_\parallel \sum_{j=1}^{L} \sum_{\sigma=\downarrow,\uparrow} \left( S^\dagger_{j+1,\sigma} S_{j,\sigma} e^\dagger_j e_{j+1} + S^\dagger_{j,\sigma} S_{j+1,\sigma} e^\dagger_{j+1} e_j \right). \tag{4.16}$$

In order to diagonalize this Hamiltonian, we proceed in a way similar to solving the $N_h = 1$ case. We begin by building states invariant in a circular permutation $Q$,

$$|\{h\}, \{\sigma\}, q\rangle = \frac{1}{\sqrt{r_\alpha}} \sum_{m=0}^{r_\alpha - 1} e^{iqm} Q^m |\{h\}, \{\sigma\}\rangle, \tag{4.17}$$

where $r_\alpha$ is the periodicity of the spin configuration $\{\sigma\}$ (labeled by $\alpha$), and

$$q = \frac{2\pi}{r_\alpha} n, \qquad n = 0, \cdots, r_\alpha - 1. \tag{4.18}$$

Again, we need to apply the Hamiltonian to the $|\{h\},\{\sigma\},q\rangle$ in order to express it in that basis. Let

$$\left|\{h'\}\right\rangle = e^\dagger_{j+1} e_j \left|\{h\}\right\rangle . \tag{4.19}$$

Applying one of the Hamiltonian's $j$-terms to state $|\{h\},\{\sigma\},q\rangle$ gives

$$\sum_\sigma S^\dagger_{j,\sigma} S_{j+1,\sigma} e^\dagger_{j+1} e_j \left|\{h\},\{\sigma\},q\right\rangle , \tag{4.20}$$

without changing the spin configuration, because a spin is exchanged with a hole, rather than exchanged with another spin. The Hamiltonian does, however, change the positions of the holes to $\{h'\}$ and moves the spin on site $j+1$ to site $j$, implying subtracting 1 to one of the $b_j$, if $j \neq L$. If $j = L$, we need to add $L-1$ to one of the $b_j$ and a phase $q$:

$$\sum_\sigma S^\dagger_{j,\sigma} S_{j+1,\sigma} e^\dagger_{j+1} e_j \left|\{h\},\{\sigma\},q\right\rangle = \left\{ \begin{array}{lll} (-1) & \left|\{h'\},\{\sigma\},q\right\rangle & \Leftarrow j \neq L \\ (-1)^{L-1} e^{iq} & \left|\{h'\},\{\sigma\},q\right\rangle & \Leftarrow j = L \end{array} \right. \tag{4.21}$$

The application of Hamiltonian 4.16 can only induce circular permutations of the spin configuration and therefore does not change the actual cyclic relative positions of the spins. This means we can discard the terms containing spin operators keeping only the hole operators, and write the Hamiltonian as

$$H_q = \sum_{j=1}^{L} t_j \left( e^\dagger_j e_{j+1} + e^\dagger_{j+1} e_j \right) , \tag{4.22}$$

where $t_{j\neq L} = -t_\parallel$ and $t_L = -t_\parallel e^{i(q-\pi L)}$.

We apply a gauge transformation like the one in the previous section, thus distributing the phase $q - \pi L$ among all $L$ sites, so that

$$t_j = -t_\parallel e^{i(q-\pi L)/L} = t_\parallel e^{iq/L}, \tag{4.23}$$

and the Hamiltonian becomes translationally invariant,

$$H_q = t_\parallel \sum_{j=1}^{L} \left( e^{iq/L} e^\dagger_{j+1} e_j + e^{-iq/L} e^\dagger_j e_{j+1} \right) , \tag{4.24}$$

reflecting the fact that, because the spin sequence remains unchanged, the system can be regarded as a set of $N_h$ independent spinless fermions on a lattice with $L$ sites. The eigenvalues are

$$E(k_1, \cdots, k_{N_h}) = 2t_\parallel \sum_{j=1}^{N_h} \cos\left( k_j - \frac{q}{L} \right) , \tag{4.25}$$

with

$$k_j = \frac{2\pi}{L} n_j \qquad n_j = 0, \cdots, L-1. \tag{4.26}$$

The eigenvalues depend only on $L$, $N_h$ and $r_\alpha$. It is important to note that this implies that all eigenstates with the same spin configuration periodicity are associated to the same eigenvalues, leading to high degeneracy. This degeneracy is lifted when the $t_\perp$ term of the Hamiltonian is considered.

## 4.3 Counting the $q$ states

An approach to the problem of counting the number of eigenstates of the $U \to \infty$ Hubbard chain which have a given momentum $q$ has already been made by Mielke [14]. Here, we present a faster method for counting how many spin configurations have a certain periodicity, which consequently shortens the time needed for solving the initial problem involving $q$. The results given by the new method are verified through comparison with Mielke's. Note that in this section, we will replace the $n$ in the definition of the momentum $q$ of the eigenstates by $j$, as explained in the next subsection.

### 4.3.1 Mielke's approach

This approach involves the Möbius function (defined in the appendix), used to invert a formula in Mielke's calculations. Let us consider a chain of $N$ spins, $N_\downarrow$ of which are down spins. The number of possible configurations is the number of $N_\downarrow$-combinations of a set of $N$ elements,

$$\begin{pmatrix} N \\ N_\downarrow \end{pmatrix} = \frac{N!}{N_\downarrow!(N-N_\downarrow)!}. \tag{4.27}$$

Out of all those possible configurations, in the general case, there are combinations with different periodicities, which are the numbers we obtain by dividing $N$ by the common divisors of $N$ and $N_\downarrow$. For example, with $N = 6$ spins and $N_\downarrow = 4$ down spins, the period of the configurations can be 6 (6/1) or 3 (6/2).

Let $f(N/d, N_\downarrow/d)$ be the number of configurations of $N/d$ spins with $N_\downarrow/d$ down spins and period $N/d$. Then, $f$ must satisfy the condition

$$\sum_{d|N,N_\downarrow} f(N/d, N_\downarrow/d) = \begin{pmatrix} N \\ N_\downarrow \end{pmatrix}. \tag{4.28}$$

Using the Möbius inversion formula, we obtain

$$f(N, N_\downarrow) = \sum_{d|N,N_\downarrow} \mu(d) \begin{pmatrix} N/d \\ N_\downarrow/d \end{pmatrix}. \tag{4.29}$$

Now that the function $f$ is well defined, we can write the number of eigenstates of the Hamiltonian with $N$ spins and $N_\downarrow$ down spins which have a given momentum

$$q = \frac{2\pi}{N} \cdot j, \tag{4.30}$$

as

$$\sum_d \frac{f(N/d, N_\downarrow/d)}{N/d}, \tag{4.31}$$

where $d$ is a divisor of $N$, $N_\downarrow$ and $j$.

### 4.3.2 A simpler approach

Let us consider a chain of N spins. The periodicity of that chain may range from 1 to $N$. Not all values are possible, though, only those that divide $N$. In order to better understand this concept, we may think of a spin chain with $N$ spins and periodicity $n$, as a set of $N/n$ equal parts with periodicity $n$. For example, a chain of length $N = 12$ could be

$$\uparrow\uparrow\downarrow\uparrow\uparrow\downarrow\uparrow\uparrow\downarrow\uparrow\uparrow\downarrow\,. \tag{4.32}$$

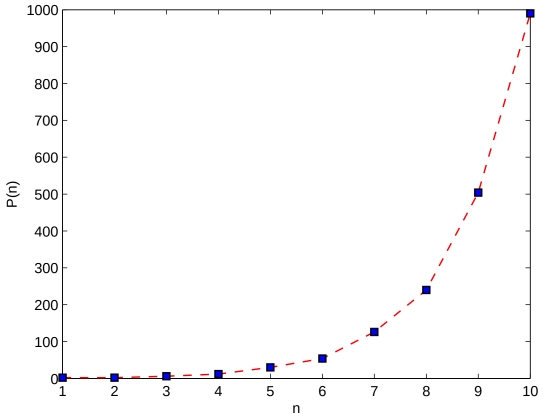

Figure 4.1: Plot of the $P(n)$ function for $n \in [1, 10]$. For each $n$, $P(n)$ gives the number of spin configurations which have period $n$.

---

Its periodicity is $n = 3$ and it is composed of $12/3 = 4$ parts

$$\uparrow\uparrow\downarrow, \tag{4.33}$$

with periodicity 3. Thus, the problem of calculating the number of possible spin configurations of a chain with $N$ spins and periodicity $n$ is reduced to that of calculating the number of spin configurations of a chain with only $n$ spins and periodicity $n$.

For example, calculating the number of spin configurations that have periodicity 3 for a chain with 90 spins is equivalent to calculating the ways in which 3 spins can be arranged to form a chain with periodicity 3. Those ways are

$$\begin{array}{ccc} \uparrow\downarrow\downarrow, & \downarrow\uparrow\downarrow, & \downarrow\downarrow\uparrow \\ \downarrow\uparrow\uparrow, & \uparrow\downarrow\uparrow, & \uparrow\uparrow\downarrow, \end{array} \tag{4.34}$$

where $\uparrow\uparrow\uparrow$ and $\downarrow\downarrow\downarrow$ are not included because their periodicity is 1. In the general case, the number of spin configurations with periodicity $n$ is 0 if $n$ does not divide $N$, and

$$P(n) = 2^n - \sum_d P(d), \tag{4.35}$$

if $n$ divides $N$. The sum involves all divisors $d$ of $n$, except for $n$ itself. The plot of this function for the first 10 values of $n$ is shown in Fig. 4.1. For large $n$, the function approaches $2^n$, so that if the $y$ axis had a logarithmic scale, we would see the line $y = \log(2)x$.

We can also represent, for each $N$, how many spin configurations exist for each possible periodicity (Fig. 4.2). Because the number of configurations increases very quickly with $n$, the logarithmic scale was used for the $y$ axis.

In the specific case of $N$ prime, spin configurations can only have periodicity 1 or $N$. The ones with periodicity 1 are $\uparrow\uparrow\uparrow\cdots$ and $\downarrow\downarrow\downarrow\cdots$; all the remaining $2^N - 2$ configurations have periodicity $N$.

Now that we know how many configurations exist for each periodicity, it becomes easier to calculate the number of eigenstates for each momentum $q$. The definition of $q$ is, again,

$$q = \frac{2\pi}{r_\alpha} j \qquad\qquad j = 0, 1, \cdots, r_\alpha - 1. \tag{4.36}$$

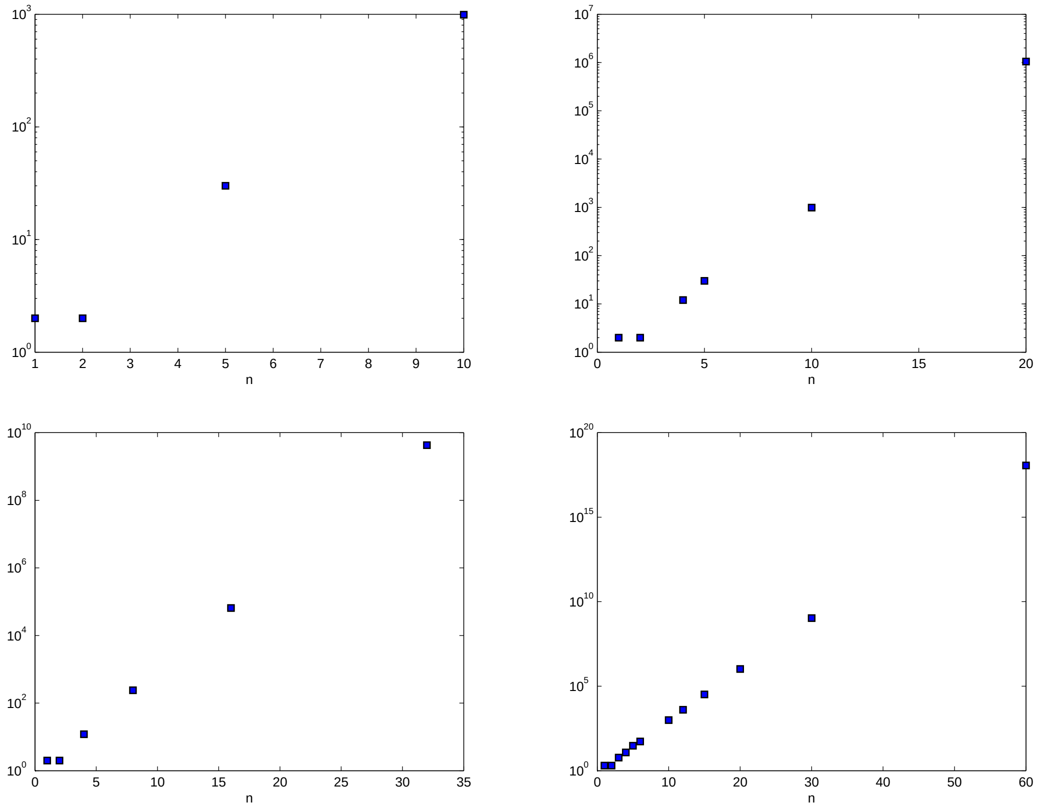

Figure 4.2: Plots of the number of possible spin configurations with periodicity $n$, for $N = 10$ (top left), $N = 20$ (top right), $N = 32$ (bottom left) and $N = 60$ (bottom right). For each $N$, it is only possible to find a spin configuration with period $n$ if $n$ is a divisor of $N$.

Let us assume, for instance, that we have $N = 6$ spins and we want to know how many eigenstates have the momentum

$$q = \frac{2\pi}{6} \cdot 4. \tag{4.37}$$

The immediate answer would be "the number of eigenstates with momentum $2\pi/6 \cdot 4$ is the number of configurations with periodicity 6, divided by 6" (we need to divide by 6 because each eigenstate is the superposition of 6 configurations that are circular permutations of each other, implying that there are less eigenstates than configurations), i. e., the answer would be

$$\frac{P(6)}{6}. \tag{4.38}$$

However, since we have

$$q = \frac{2\pi}{6} \cdot 4 = \frac{2\pi}{3} \cdot 2, \tag{4.39}$$

there are $P(3)/3$ eigenstates made up of configurations with periodicity 3 which can also have this momentum value. Therefore, in the general case, if the number of spins is $N$, the number of eigenstates with momentum

$$q = \frac{2\pi}{N} \cdot j \tag{4.40}$$

is

$$\sum_g \frac{P(N/g)}{N/g}, \tag{4.41}$$

where the possible values of $g$ are the common divisors of $N$ and $j$. If we add the result of expression 4.31 for all $N_\downarrow = 0, 1, \cdots, N$, we obtain the result given by 4.41, as long as

$$\sum_{N_\downarrow} f(N, N_\downarrow) = P(N). \tag{4.42}$$

We can verify this equality by plotting

$$\frac{\sum\limits_{N_\downarrow} f(N, N_\downarrow)}{P(N)}, \tag{4.43}$$

for some values of $N$. Fig. 4.3 shows the resulting plot, providing a confirmation that Mielke's approach gives the same result as ours.

### 4.3.3 Results

Fig. 4.4 shows the number of eigenstates for each value of $q$ (recall $q = 2\pi/(N) \cdot j$, with $j = 0, \cdots, N-1$), for different lengths of the spin chain. In some plots, the scale of the vertical axis shows the same value for all points. This is a precision issue, due to the fact that, for $N$ greater than 20, the difference between the maximum and minimum number of eigenstates is tens of orders of magnitude lower than the number of eigenstates itself (of the order of $2^N$). Nevertheless, it can still be easily seen that the values of $q$ with the most eigenstates are those whose respective $j$ is a multiple of some divisor of $N$.

Fig. 4.5 shows the difference between the number of eigenstates for each value of $q$ and the minimum value, for 4 different $N$. The values of $N$ used here were 40, 60, 80, 100, in order to simulate the thermodynamic limit. The plots show that, as $N$ increases, the difference

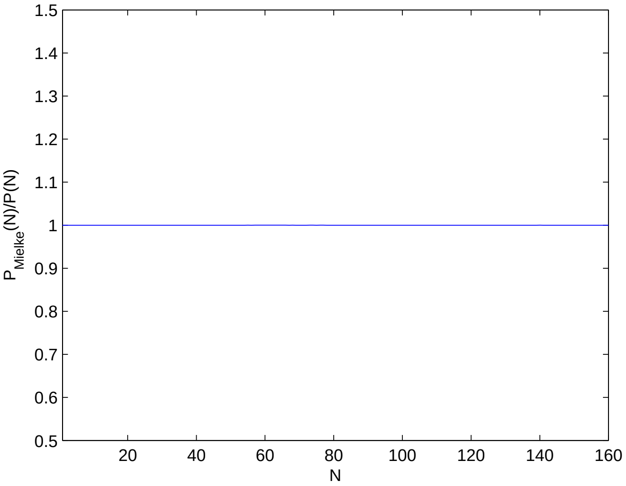

Figure 4.3: Plot of the quotient between the number of states with periodicity $N$ given by Mielke's formula and our formula. The results obtained using Mielke's formula were computed in 8.2 seconds, while ours took only 0.1 seconds.

between the maximum and minimum values for the number of states increases at a high rate. Prime numbers also follow this pattern, but their respective plots are all similar to that of $N = 23$.

From all of the plots presented, one realizes that, as we approach the thermodynamic limit, the plotted function,

$$N_s(N, q) = \sum_g \frac{P(N/g)}{N/g} \approx \frac{2^N}{N}, \tag{4.44}$$

which is an expression that does not depend on $q$, justifying the numerical difficulty of representing this function.

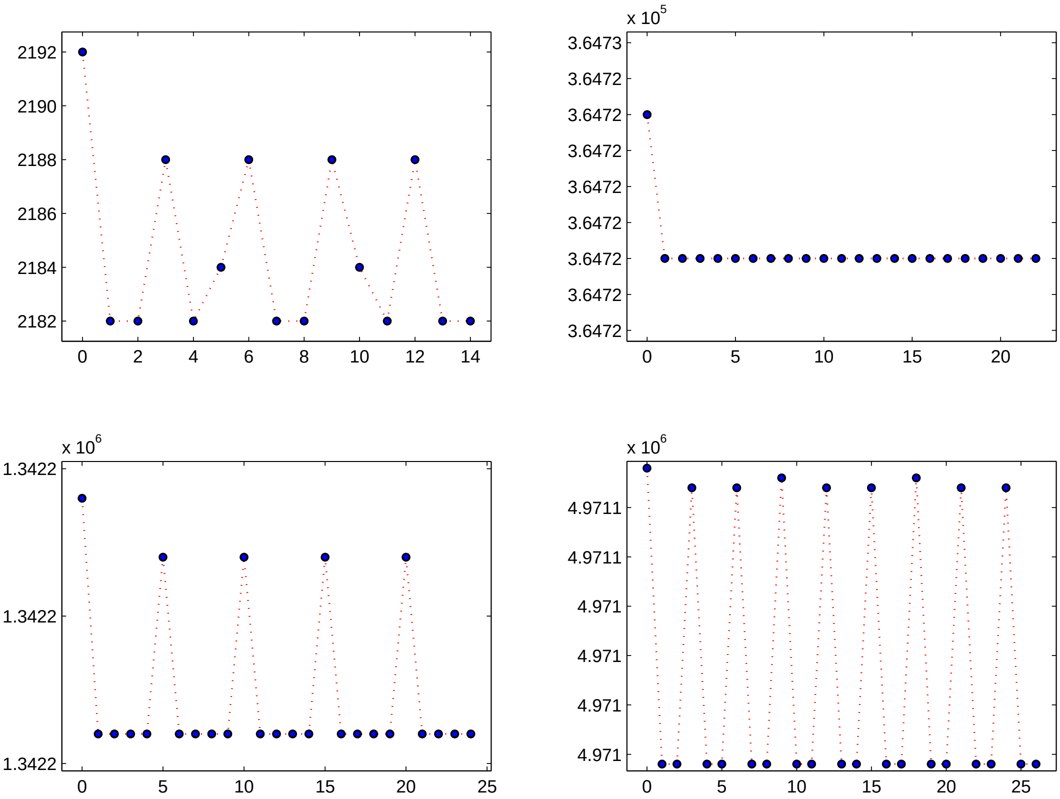

Figure 4.4: Representation of the number of eigenstates of 4.24 as a function of $j$, that is, of $qN/(2\pi)$, for $N = 15$ (top left), $N = 23$ (top right), $N = 25$ (bottom left) and $N = 27$ (bottom right).

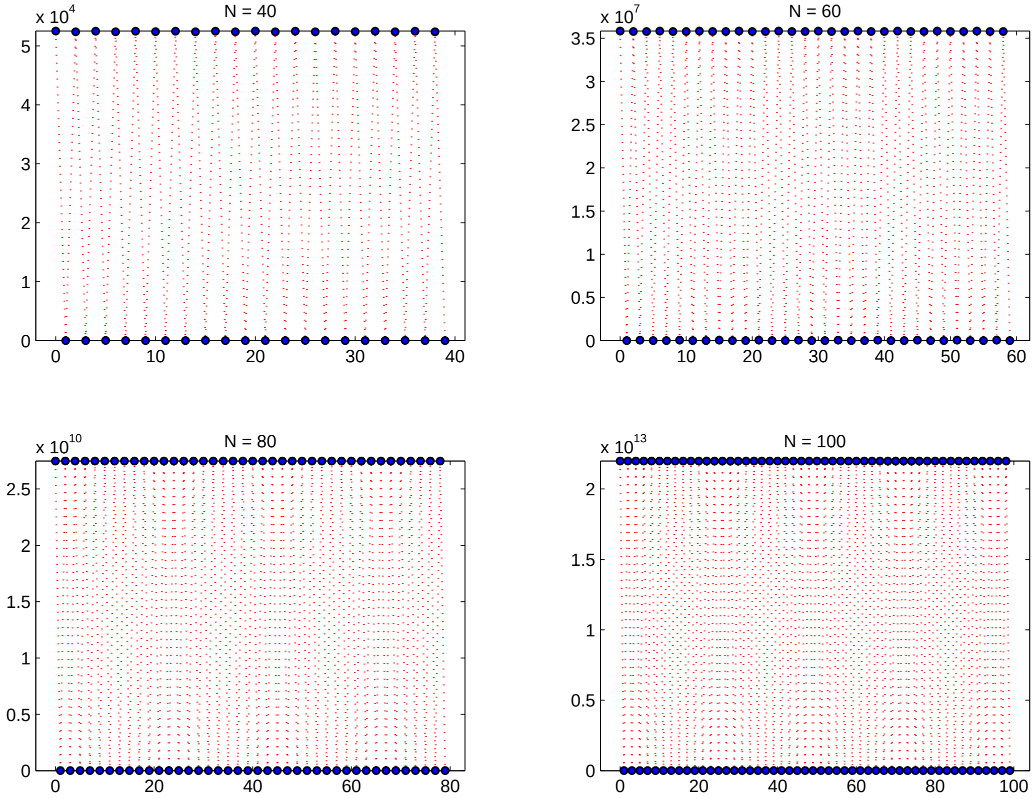

Figure 4.5: Representation of the difference between the number of eigenstates of 4.24 and its minimum value, as a function of $j$, that is, of $q = 2\pi/(N) \cdot j$, for $N = 40$ (top left), $N = 60$ (top right), $N = 80$ (bottom left) and $N = 100$ (bottom right). The minimum value has been subtracted on each plot, lest the program assume all values are identical.

## 4.4 Thermodynamics

Using the results from the last subsections, one easily calculates thermodynamic functions of the helicoidal Hubbard model in the strong-coupling limit with $t_\perp = 0$. We begin by defining the partition function $Z$ as

$$Z = \sum_r e^{-E_r/(k_B T)}, \tag{4.45}$$

where $r$ labels all possible states of the system.

We know that no more than one hole can occupy each $k$ state. This implies that each of the $N_h$ holes can have any value of $k$ as long as no other hole has it. Therefore, the number of eigenstates the holes can occupy is obtained by counting the number of combinations of $N_h$ values that can be extracted from the list of $L$ possible values of $k$, that is, $\binom{L}{N_h}$.

For the $N = L - N_h$ spins, we know from the previous subsection that the number of states with spin momentum $q$ is given by the function $N_s(N, q)$.

The partition function can be numerically calculated for fixed $L$ and $N_h$ using the expression

$$Z = \sum_{\{k\}} \sum_q N_s(N, q) e^{-E(\{k\})/(k_B T)}, \tag{4.46}$$

where:

- the first summation is taken over all the different combinations of $N_h$ values of $k$;
- the second summation is taken over $q = 2\pi/N \cdot j$ with $j = 0, \cdots, N-1$ (the counting of the spin periodicities that are divisors of $N$ is included in $N_s(N, q)$);
- the energy eigenvalues are $E(\{k\}) = 2t_\parallel \sum_{i=1}^{N_h} \cos\left(k_i - \frac{q}{L}\right)$.

The partition function was used to calculate the thermodynamic energy,

$$\langle E \rangle = -\frac{\partial \ln Z}{\partial \beta}, \tag{4.47}$$

the heat capacity,

$$C_v = \frac{\partial \langle E \rangle}{\partial T}, \tag{4.48}$$

and the entropy of the system,

$$S = \frac{\partial}{\partial T} \left( k_B T \ln Z \right), \tag{4.49}$$

as a function of $k_B T$.

### Energy

Figure 4.6 shows a few plots of the energy as a function of $k_B T$, each corresponding to $N_h = 1, \cdots, 5$, and fixed $L = 10$. It can be seen that, as the number of holes increases, the energy decreases. Additionally, we see that for high $T$, the energy goes to 0, which is explained by the fact that holes and particles have the same probability of occupying a state. There are as many positive eigenvalues as there are negative ones, thus their average is zero.

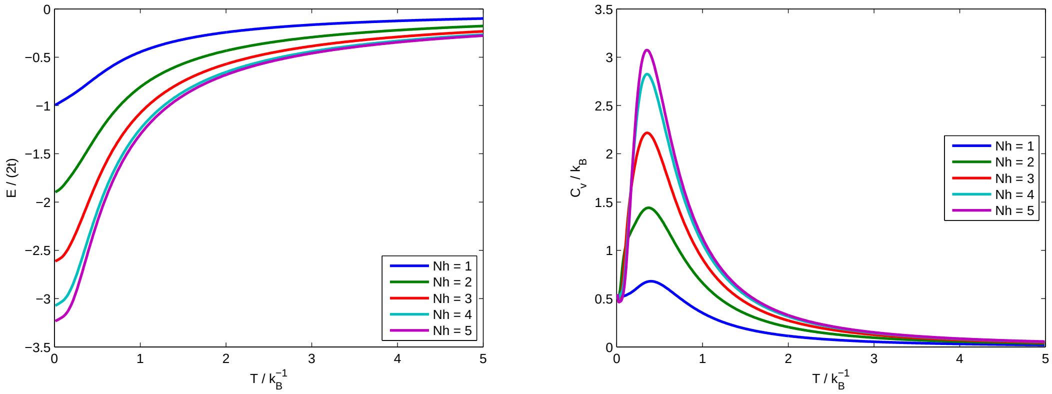

Figure 4.6: Average energy $\langle E \rangle$ (left) and heat capacity $C_v$ (right) of the strong-coupling helicoidal Hubbard model in the $t_\perp = 0$ limit, with $L = 10$. The plots for $N_h$ and for $L - N_h$ are identical, due to particle-hole symmetry of Hamiltonian 4.24.

---

### Heat capacity

Figure 4.6 contains plots of the heat capacity as a function of $k_B T$, for $L = 10$ and different values of $N_h$, ranging from 1 to 5. Both on the $C_v$ and $\langle E \rangle$ plots, particle-hole symmetry is present (the Hamiltonian 4.24 has particle-hole symmetry), so that the functions $C_v(T)$ or $\langle E \rangle(T)$ for have the same expression for $N_h$ and $L - N_h$.

### Entropy

The entropy $S(T)$ (Fig. 4.7) is the thermodynamic function whose analysis is the most interesting one. The symmetry present in the previous two functions is not valid anymore. In fact, as $S$ is a measure of the number of available states, it changes when a spin is replaced by a (spinless) hole.

For $T \to \infty$, all states are equally probable, and we can calculate the entropy analytically in this limit. The number of states accessible to the $N_h$ holes is $\binom{L}{N_h}$ and the number of states accessible to the spins is $2^N$, therefore

$$S(T \to \infty)/k_B = \ln\left(\frac{L!}{N_h! N!} 2^N\right), \tag{4.50}$$

which is a result confirmed by the plots in figure 4.7. Another effect that can be seen from the plots is the fact that, for low $T$, more holes mean lower entropy. The holes occupy the $k$ states which lead to lowest energies. However, for high $T$, the system with the highest $N_h$ is no longer the one with the highest entropy. This occurs because $S_\infty(N_h)$ has a maximum, which can be calculated analytically, using Stirling's approximation $\ln N! \approx N \ln N - N$, allowing the approximation of

$$\frac{dS_\infty(N_h)}{dN_h} = k_B \frac{d}{dN_h} \ln\left(\frac{L!}{N_h!(L-N_h)!} 2^{L-N_h}\right), \tag{4.51}$$

to

$$\frac{1}{k_B}\frac{dS_\infty(N_h)}{dN_h} \approx -\ln 2 + \frac{d}{dN_h}\left(-N_h \ln N_h + N_h - (L-N_h)\ln(L-N_h) + (L-N_h)\right); \tag{4.52}$$

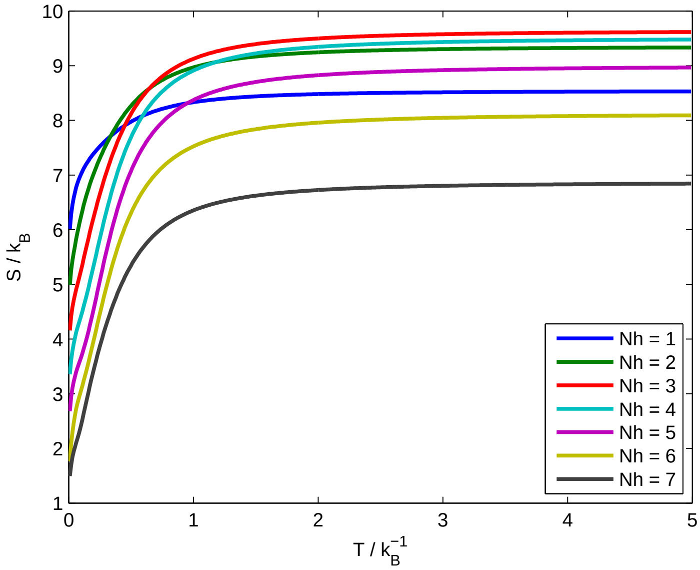

Figure 4.7: Entropy $S$ of the strong-coupling helicoidal Hubbard model in the $t_\perp = 0$ limit, with $L = 10$. For high $T$, the maximum entropy occurs for $N_h = L/3$ rounded to the nearest integer which, in this case, is 3.

the equation $\frac{dS_\infty(N_h)}{dN_h} = 0$ has only one solution,

$$N_h = \frac{L}{3}. \tag{4.53}$$

This is the solution for continuous $N_h$. For our discrete case, the maximum will occur for $L/3$ rounded to the nearest integer. For $L = 10$ (Fig. 4.7), that integer is 3, providing the reason why the plot of $S$ for $N_h = 3$ has the highest value when $T \to \infty$.

Let us now study what happens to the entropy when we only allow ferromagnetic states ($r_\alpha = 1$). The lattice is now made of $N_h$ holes and $L - N_h$ equal spins, which implies particle-hole symmetry is present once again, because the spin chain is only allowed two states ($\uparrow\uparrow\uparrow\cdots$ and $\downarrow\downarrow\downarrow\cdots$), independently of the number of spins. Figure 4.8 shows the entropy $S(T)$ for lattices with 9 (top) and 10 (bottom) sites. In the $T \to \infty$ limit, the entropy goes to

$$\begin{aligned} S_\infty &= k_B \ln(\text{number of spin states} \times \text{number of hole states}) \\ &= k_B \ln\left[2\binom{L}{N_h}\right] \\ &= k_B \ln\left[2\frac{L!}{N_h!(L-N_h)!}\right] \end{aligned} \tag{4.54}$$

independently of the parity of $L$ and $N_h$.

However, in the $T \to 0$ limit, the spins will still have only 2 allowed states, while the holes may have 1 or 2 ground $k$ states. Let us recall the definition of the momentum of the holes,

$$k = \frac{2\pi}{L}n \qquad n = 0, \cdots, L-1. \tag{4.55}$$

Regarding this definition,

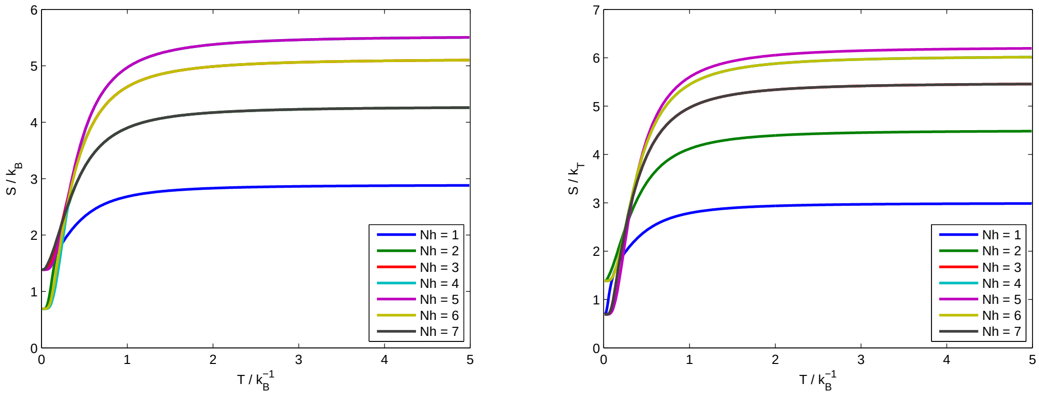

Figure 4.8: Entropy of the ferromagnetic strong-coupling helicoidal Hubbard model in the $t_\perp = 0$ limit, for $L$ odd (9, left) and even (10, odd). In this limit, entropy shares the particle-hole symmetry with the average energy and the heat capacity, because only two states are allowed to the spin chain, independently of its length.

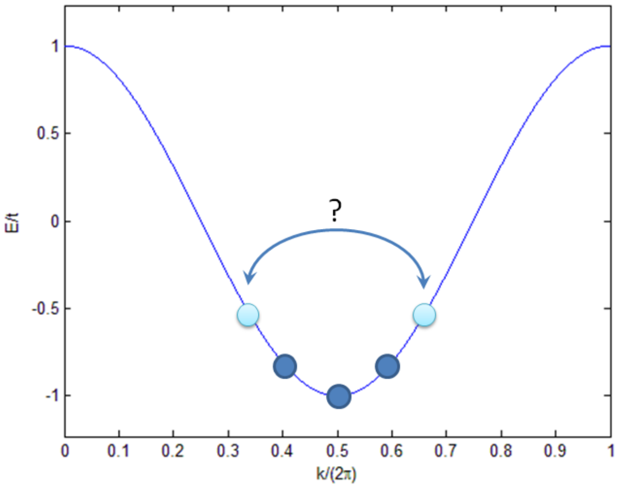

Figure 4.9: Representation of the hole energy band for a lattice with an arbitrary even number of sites, considering the strong-coupling helicoidal Hubbard model in the $t_\perp = 0$ limit. In such a lattice, all $k$ states except $k = \pi$ are degenerate, and that degeneracy is relevant when the number of holes if even (4, in this plot).

- the ground state $k = \pi$ is only allowed for $L$ even. If the number of holes is odd, one of them will occupy the bottom of the band, and the rest will fill it in pairs, symmetrically, meaning the ground state of the holes is unique. If the number of holes is even, one hole will remain after symmetrically filing up the states; this hole can either occupy the "left" or the "right" lowest free state in the band (figure 4.9), leading to a doubly degenerate global ground state;
- for an odd $L$, holes can no longer occupy the $k = \pi$ state. Consequently, there are two band states with the lowest energy. Unlike what happens for $L$ even, an even number of holes can only occupy one global ground state, while an odd number of holes has two possibilities for its global ground state.

These results for the ferromagnetic configuration are summarized in the following table (where $S$ is in $k_B$ units):

| | | $S(T = 0)$ | $S(T \to \infty)$ |
|---|---|---|---|
| $L$ even | $N_h$ even | $\ln 4$ | $\ln(2 \times \binom{L}{N_h})$ |
| | $N_h$ odd | $\ln 2$ | $\ln(2 \times \binom{L}{N_h})$ |
| $L$ odd | $N_h$ even | $\ln 2$ | $\ln(2 \times \binom{L}{N_h})$ |
| | $N_h$ odd | $\ln 4$ | $\ln(2 \times \binom{L}{N_h})$ |

For example, the entropy of the ferromagnetic strong-coupling helicoidal Hubbard model with an even number of sites ($L$) and an odd number of holes ($N_h$) at $T = 0$ is $\ln 2$.

# Chapter 5

# The quantum spin queue model

In this chapter, the effect of a finite $t_\perp$, such that $U \gg t_\parallel \gg t_\perp \gg t_\parallel^2/U$, will be considered (in first order perturbation). The effect of this term is to partially lift the spin degeneracy. We first diagonalize the $t_\perp$ term of the Hamiltonian of the helicoidal model with one hole and one different spin in order to introduce the $\Delta$-permutation operator. This operator leads to *spin queue* whose dynamics gives the solution of the tight-binding helicoidal Hubbard Hamiltonian in this limit.

## 5.1 The $t_\perp \neq 0$ limit with one hole and one up spin

In the Hamiltonian of the helicoidal Hubbard model in the strong coupling limit,

$$\begin{aligned} H = \quad & -t_\parallel \sum_{j,\sigma}(1-n_{j,\bar\sigma})c^\dagger_{j,\sigma}c_{j+1,\sigma}(1-n_{j+1,\bar\sigma}) + \text{h.c.} \\ & -t_\perp \sum_{j,\sigma}(1-n_{j,\bar\sigma})c^\dagger_{j,\sigma}c_{j+\Delta,\sigma}(1-n_{j+\Delta,\bar\sigma}) + \text{h.c.}, \end{aligned} \tag{5.1}$$

$t_\parallel$ induces a permutation in the spin configuration if the hole does a full loop along the helix, while one single hop across helix pitches due to $t_\perp$ is enough to induce such a permutation. In the strong coupling limit, these permutations are easier to be treated if we consider all of the spins have the same orientation except for one, so that the spin configuration states can be labeled using only one number: the position of the different spin.

### 5.1.1 The $\Delta$-permutation operator

Let us consider an invariant state $|j,\{\sigma\},q\rangle = |q\rangle$ as defined in 4.4. Considering the one-site translation operator $Q$ defined earlier, one obtains, for an arbitrary operator $\hat{A}_i$ acting upon site $i$,

$$\langle q|\,\hat{A}_i\,|q\rangle = \langle q|\,Q^{-1}Q\hat{A}_iQ^{-1}Q\,|q\rangle\,. \tag{5.2}$$

Since

$$\begin{aligned} &\langle q|\,Q^{-1} = e^{iq}\,\langle q|\,, \\ &Q\,|q\rangle = e^{-iq}\,|q\rangle\,, \\ &Q\hat{A}_iQ^{-1} = \hat{A}_{i+1}, \end{aligned} \tag{5.3}$$

we conclude that

$$\langle q|\,\hat{A}_i\,|q\rangle = \langle q|\,\hat{A}_{i+1}\,|q\rangle\,. \tag{5.4}$$

It immediately follows that

$$\langle q|\,\hat{A}_i\,|q\rangle = \frac{1}{N}\,\langle q|\sum_{i=1}^{N}\hat{A}_i\,|q\rangle\,. \tag{5.5}$$

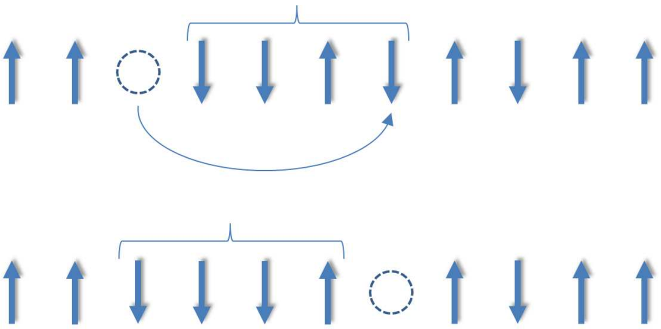

Figure 5.1: When the hole jumps from site $i$ to site $i+\Delta$, it induces a circular permutation of the spins between sites $i+1$ and $i+\Delta$.

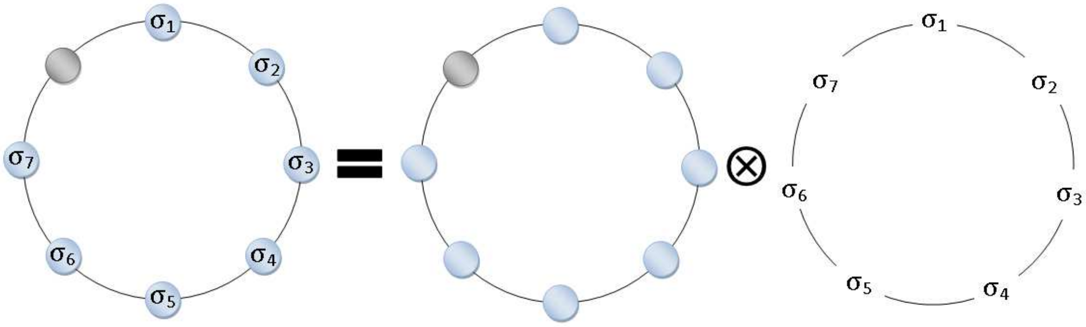

Figure 5.2: A ring or helix with one hole and particles with spin can be regarded as the tensorial product of a ring with one free hole and a ring with spins only.

Let us introduce the $\Delta$-permutation operator $Q_{i,i+\Delta}$ [15] whose action upon the spin configuration is equivalent to the hopping of the hole from site $i$ to site $i+\Delta$. For example, if the hole hops from site 1 to site 5, we can write the action of the permutation operator as

$$Q_{1,5}\left|\sigma_1,\sigma_2,\sigma_3,\sigma_4,\sigma_5,\sigma_6,\sigma_7\right\rangle = \left|\sigma_4,\sigma_1,\sigma_2,\sigma_3,\sigma_5,\sigma_6,\sigma_7\right\rangle, \tag{5.6}$$

Therefore, assuming $\hat{A}_i$ is the $\Delta$-permutation operator $Q_{i,i+\Delta}$, the average value

$$\langle j,\{\sigma\},q|\, Q_{i,i+\Delta}\, |j,\{\sigma\},q\rangle \tag{5.7}$$

is the same for any $i$ and

$$\langle j,\{\sigma\},q|\, Q_{i,i+\Delta}\, |j,\{\sigma\},q\rangle = \frac{1}{N}\langle j,\{\sigma\},q| \sum_{i=1}^{N} Q_{i,i+\Delta}\, |j,\{\sigma\},q\rangle\,, \tag{5.8}$$

where $N$ is the number of spins.

### 5.1.2 The effect of $t_\perp$ in the spin configurations

The $t_\perp$ term of the Hamiltonian has two effects upon the states: it changes both the position of the hole and the spin configuration of the helix. This is illustrated in Fig. 5.1.

Thus, we can rewrite $(1-n_{j,\bar{\sigma}})c^\dagger_{j,\sigma}c_{j+\Delta,\sigma}(1-n_{j+\Delta,\bar{\sigma}})$ when acting on a state $|j,\{\sigma\},q\rangle$ as (see Fig. 5.2)

$$(1-n_{j,\bar{\sigma}})c^\dagger_{j,\sigma}c_{j+\Delta,\sigma}(1-n_{j+\Delta,\bar{\sigma}}) \rightarrow e^\dagger_{j+\Delta}e_j \otimes \frac{1}{N}\sum_{j=1}^{N} Q_{j,j+\Delta}. \tag{5.9}$$

The position of the hole is changed by applying $e^\dagger_{j+\Delta}e_j$ and the spin configuration is changed by the permutation operator $Q_{i,i+\Delta}$. Solving both these terms gives the solution of the helicoidal Hubbard model in the limit defined above. In the following subsections, the solution with one hole and one different spin is presented.

### 5.1.3 The hole hopping term

In the previous subsection, we separated the $t_\perp$ terms of the Hamiltonian in a product of two: $H_h$, the term with one hole and empty sites, and $H_s$, the term with spins and no hole. The first of those terms (considering only the hole hopping to the right, for example) reads

$$H_h = t_\perp \sum_{j=1}^{L} e^\dagger_{j+\Delta}e_j, \tag{5.10}$$

where $L$ is the number of sites on the helix and $e^\dagger_j$ is the creation operator of the hole on site $j$. Clearly, this Hamiltonian is a simple tight-binding one, with hopping range $\Delta$ instead of the usual nearest neighbor range. The eigenstates of $t_{||}$ are also eigenstates of this term. In the case of one hole,

$$|k_h\rangle = \frac{1}{\sqrt{L}}\sum_{j=1}^{L} e^{ik_h j}|j\rangle, \tag{5.11}$$

with

$$k_h = \frac{2\pi n}{L} \qquad n = 0, \cdots, L-1, \tag{5.12}$$

and the eigenvalues are

$$t_\perp e^{-ik_h\Delta}. \tag{5.13}$$

In this explanation, we have not included the phases due to the gauge transformation of section 4.2. These will be considered in the following sections.

### 5.1.4 The spin exchange term

The second Hamiltonian term associated with the previous one, from the splitting in 5.9, is

$$H_s = \sum_{j=1}^{N} Q_{j,j+\Delta}, \tag{5.14}$$

where $N = L-1$ is the number spins and again, only the hole hopping "to the right" ($j \rightarrow j+\Delta$) is being considered. In order to solve this part of the Hamiltonian, we shall forget about the hole and consider only the spin configuration. The states $|j\rangle$ will be labeled according to the position $j$ of the different spin ($\uparrow$) in the chain. For example, for $N=6$:

$$|\downarrow\downarrow\uparrow\downarrow\downarrow\downarrow\rangle = |j=3\rangle. \tag{5.15}$$

Applying the operator $Q_{4,6}$ to this state will change the spin configuration in the same way as if there was a hole on site 4, and that hole hopped to site 6. The operator $Q_{4,6}$ was chosen so that its application to the state mentioned does not change it, because the ↑ spin will still be in position 3. If we applied $Q_{5,3}$ instead, we would be simulating the hopping of the hole from site 5 to site 3, so that the ↑ spin will now be in position $j = 4$:

$$Q_{5,3} \left| j = 3 \right\rangle = \left| j = 4 \right\rangle . \tag{5.16}$$

When the Hamiltonian acts upon a state $\left| j \right\rangle$, it simulates all possible hoppings of the hole. One of them involves the hole exchanging with the ↑ spin, so that the resulting state is

$$\left| j - \Delta + 1 \right\rangle . \tag{5.17}$$

When the jump of the hole makes a ↓ spin go from the right to the left of the ↑ spin, we obtain

$$\left| j + 1 \right\rangle . \tag{5.18}$$

The number of $Q$ operators that make the hole perform such a jump is $\Delta - 1$. If the hole hops in any other way, the state is not changed.

To sum up, applying $H_s$ to a state $\left| j \right\rangle$ gives

$$H_s \left| j \right\rangle = \left| j - \Delta + 1 \right\rangle + (\Delta - 1) \left| j + 1 \right\rangle + (N - \Delta) \left| j \right\rangle . \tag{5.19}$$

The eigenstates of $H_s$ in this subspace with one inverted spin are given by a superposition of the basis states $\left| j \right\rangle$,

$$\left| q \right\rangle = \frac{1}{\sqrt{N}} \sum_{j=1}^{N} e^{iqj} \left| j \right\rangle , \tag{5.20}$$

and the eigenvalues are found by applying the Hamiltonian to these states:

$$\begin{aligned} H_s \left| q \right\rangle &= \tfrac{1}{\sqrt{N}} \sum_j e^{iqj} \left[ \left| j - \Delta + 1 \right\rangle + (\Delta - 1) \left| j + 1 \right\rangle + (N - \Delta) \left| j \right\rangle \right] \\ &= \left[ e^{iq(\Delta - 1)} + (\Delta - 1) e^{-iq} + N - \Delta \right] \left| q \right\rangle , \end{aligned} \tag{5.21}$$

which, recalling $q = 2\pi n / r_\alpha = 2\pi n / N$, because we have only one up spin, gives the eigenvalues

$$\exp\left( i(\Delta - 1) \frac{2\pi n}{N} \right) + (\Delta - 1) \exp\left( -i \frac{2\pi n}{N} \right) + N - \Delta \tag{5.22}$$

Combining the results 5.13 and 5.22, we obtain

$$E_{k_h,q} = t_\perp \left( e^{-ik_h \Delta} \left( e^{iq(\Delta-1)} + (\Delta - 1) e^{-iq} + N - \Delta \right) + \text{h.c.} \right) \tag{5.23}$$

## 5.2 The $t_\perp \neq 0$ limit with $N_h$ holes

Having solved the $t_\perp = 0$ limit with $N_h$ holes allows a few immediate simplifications of the $t_\perp$ term. The energy correction due to this term lifts the degeneracy of the eigenvalues in 4.26.

The $t_\perp$ term of the Hamiltonian is

$$H_\perp = -t_\perp \sum_{j,\sigma} (1 - n_{j,\bar{\sigma}}) c^\dagger_{j,\sigma} c_{j+\Delta,\sigma} (1 - n_{j+\Delta,\bar{\sigma}}) + \text{h.c.}, \tag{5.24}$$

which, using slave-fermion notation, is written as

$$H_\perp = t_\perp \sum_{j,\sigma} e^{-i(q/L-\pi)\Delta} S^\dagger_{j+\Delta,\sigma} S_{j,\sigma} e^\dagger_j e_{j+\Delta} + \text{h.c.} \tag{5.25}$$

where the gauge transformation which distributes the $q - \pi L$ phase among all sites has been considered, so that $(q/L - \pi)\Delta$ is the phase loss when an electron jumps from site $j$ to site $j + \Delta$.

Let us consider the helix configuration

$$\uparrow\uparrow\downarrow\, 0 \uparrow 0 \downarrow\downarrow\uparrow 0 \uparrow\downarrow, \tag{5.26}$$

where 0 represents an empty site. If $\Delta = 4$, the jump of the spin on site 2 to site 6 on this helix configuration corresponds to the jump of spin 2 to site 4 on the spin configuration (called the *squeezed spin chain*). The difference (6-4) is due to the hole that spin 2 had to jump over.

In the general case, the jump

$$j \to j + \Delta, \tag{5.27}$$

on the helix configuration, corresponds to the jump

$$j' \to j' + \Delta', \tag{5.28}$$

on the squeezed spin chain, where $j'$ depends on the number of holes to the left of site $j$, and $\Delta'$ is a function of the number of holes between sites $j$ and $j + \Delta$. When there are $N_h$ holes between sites $j$ and $j + \Delta$, then $\Delta' = \Delta - 1 - N_h$.

The condition $t_\perp = 0$ turns the helix into a ring, as mentioned before, and a ring has $\Delta = 1$. In the $t_\perp = 0$ limit studied in the previous chapter, all jumps had $\Delta = 1$ and $N_h = 0$, implying $\Delta' = 0$. This is another way to understand why the squeezed spin chain always remained unchanged.

Just like what happened with one hole and one different spin, the jump

$$i \to i + \Delta \tag{5.29}$$

makes the spins between sites $i'$ and $i' + \Delta' + 1$ jump one site to the left (on the squeezed spin chain). This is the quantum spin queue model: spins jump a certain number of sites in a given direction, and all spins between the initial and final sites are pushed one site in the opposite direction, inducing a circular permutation of the configuration formed by these spins (see Fig. 5.1).

This jump can therefore be written as

$$e^\dagger_i e_{i+\Delta} S^\dagger_{i+\Delta,,\sigma} S_{i,\sigma} = e^\dagger_i e_{i+\Delta} \sum_{n_h=0}^{\Delta-1} P_{i,i+\Delta}(n_h) Q_{i',i'+\Delta'}, \tag{5.30}$$

where $n_h$ is the number of holes between sites $i$ and $i + \Delta$; if there are less holes on the system than $\Delta - 1$, then the sum is taken only up to the number of holes $N_h$. Additionally,

$$P_{i,i+\Delta}(n_h) = \sum_{\{b\}} \left[ \prod_{j=1}^{n_h} n_{i+b_j} \prod_{j=n_h+1}^{\Delta-1} (1 - n_{i+b_j}) \right], \tag{5.31}$$

is a projection operator which imposes there are $n_h$ holes between sites $i$ and $i+\Delta$; the sum is calculated over the number of $n_h$-combinations of a set of $\Delta-1$ elements, $\binom{\Delta-1}{n_h}$, and $n_b = e_b^\dagger e_b$ is the number of holes on site $b$ (0 or 1).

The permutation operator $Q_{i',i'+\Delta'}$ can be written as [15]

$$Q_{i',i'+\Delta'} = \prod_{j=i'}^{i'+\Delta'} \left(2S_j \cdot S_{j+1} + \frac{1}{2}\right). \tag{5.32}$$

Replacing 5.30 in the Hamiltonian 5.25 gives

$$H_\perp = t_\perp \sum_{j,\sigma} e^{-i(q/L-\pi)\Delta} e_j^\dagger e_{j+\Delta} \sum_{n_h=0}^{\Delta-1} P_{j,j+\Delta}(n_h) \sum_{j'=1}^{L-n_h} \frac{1}{L-n_h} Q_{j',j'+\Delta'} + \text{h.c.} \tag{5.33}$$

In order to determine the first order energy corrections due to this term, we have to evaluate

$$\left\langle \{k\},\{\sigma'\},q \right| H_\perp \left|\{k\},\{\sigma\},q\right\rangle, \tag{5.34}$$

where $\{k\}$ is the set that includes the value of $k$ for every hole. The terms of the sum over $n_h$ can be factorized and we obtain

$$\begin{aligned} &\langle \{k\},\{\sigma'\},q| H_\perp |\{k\},\{\sigma\},q\rangle = \\ &\sum_{n_h} [\langle \{k\}| \sum_{j,\sigma} t_\perp e^{-i(q/L-\pi)\Delta} e_j^\dagger e_{j+\Delta} P_{j,j+\Delta}(n_h) |\{k\}\rangle \\ &\times \langle \{\sigma'\},q| \tfrac{1}{L-N_h} \sum_{j'=1}^{L-N_h} Q_{j',j'+\Delta'} |\{\sigma\},q\rangle] + \text{h.c.} \end{aligned} \tag{5.35}$$

where the summation over $n_h$ goes from $n_h = 0$ to $n_h = \min(N_h-1, \Delta-1)$, reflecting the fact that the total number of holes may be less than $\Delta - 1$ (the maximum number of holes that can be present between sites $i$ and $i+\Delta$, as mentioned above). So we have reduced the helicoidal Hubbard model to a Hubbard chain plus a correction (spin queue model ⊗ hole correlation function).

We now need to calculate the average value

$$\langle e_i^\dagger e_{i+\Delta} P_{i,i+\Delta}(n_h)\rangle = \sum_{\{b\}} \langle e_i^\dagger e_{i+\Delta} \prod_{j=1}^{n_h} n_{i+b_j} \prod_{j=n_h+1}^{\Delta-1} (1 - e_{i+b_j}^\dagger e_{i+b_j})\rangle \tag{5.36}$$

In Appendix A, we show how these averages can be calculated. We will now present the final energy dispersion for the case of one hole.

### 5.2.1 The $N_h = 1$ case

If the system has only one hole, that hole must be on site $i+\Delta$, for the jump $i \to i+\Delta$ to occur, meaning there are no holes between sites $i$ and $i+\Delta$, and $n_h = 0$. Then, both products in 5.36 simplify to 1, and the average value simplifies to

$$\sum_{\{b\}} \langle e_i^\dagger e_{i+\Delta}\rangle. \tag{5.37}$$

Since we have $n_h = 0$, then $\binom{\Delta-1}{n_h} = 1$, and

$$\langle e_i^\dagger e_{i+\Delta} P_{i,i+\Delta}(n_h) \rangle = \frac{1}{L} e^{ik_h \Delta}, \tag{5.38}$$

allowing us to write the matrix element $\langle \{k\}, \{\sigma'\}, q| H_\perp |\{k\}, \{\sigma\}, q\rangle$ as

$$\frac{t_\perp}{N} e^{i\Delta(k_h+\pi-q/L)} \sum_{j'=1}^{N} \langle Q_{j',j'+\Delta} \rangle, \tag{5.39}$$

where $N = L - 1$ is the number of spins. Inserting the solution 5.22 for one inverted spin, the matrix elements finally become

$$\frac{t_\perp}{N} e^{i\Delta(k_h+\pi-q/L)} \left( e^{iq(\Delta-1)} + (\Delta-1)e^{-iq} + N - \Delta \right) + \text{h.c.}, \tag{5.40}$$

corresponding to the eigenvalues of the Hamiltonian,

$$\frac{2t_\perp}{N} \left\{ \cos[\Phi\Delta](N-\Delta) + \cos[\Phi - q](\Delta - 1) + \cos[\Phi + (\Delta-1)q] \right\}, \tag{5.41}$$

where $\Phi = k_h + \pi - q/L$.

# Chapter 6

# Spectral function

As an example of application of the results from the previous chapters, we can calculate the spectral function. The spectral function is directly obtained when performing an Angle Resolved Photoemission Spectroscopy (ARPES) experiment. This technique probes both the momentum and energy of electrons on a material, usually a solid. Standard photoelectric effect measures only the energy of electrons in metals, by impinging monochromatic light upon the material, and measuring the energy of the ejected electrons. This provides us with information on the distribution of the electrons of the metal among the allowed energy levels. If we measure not only distribution of energies but also that of angles, we obtain information about the electrons' momenta. Spectral functions include all this information. In particular, it has been an important tool to probe spin-charge separation in quasi unidimensional metals and the pseudo-gap regime in high temperature superconductors [16].

In this chapter, known results for the $U \to \infty$ Hubbard chain at half-filling are used to generate the spectral function of the helicoidal Hubbard model with $t_\perp = 0$ (work still in progress).

## 6.1 1D Hubbard model

The spectral function of a system can be calculated from the Green's function $G(k, \omega)$ of that system, given by

$$G(k,\omega) = \left\langle \Psi^0 \right| c^\dagger_{k\uparrow} (\omega + E_0 - H - i\delta)^{-1} c_{k\uparrow} \left| \Psi^0 \right\rangle, \tag{6.1}$$

for the $U \to \infty$ Hubbard model with one hole, where $\left|\Psi^0\right\rangle$ is the nondegenerate ground-state wave function of the undoped system and $E_0$ is its respective energy. From $G(k, \omega)$, the spectral function $A(k, \omega)$ is obtained simply by computing

$$A(k,\omega) = \frac{1}{\pi} \text{Im } G(k,\omega). \tag{6.2}$$

Parola and Sorella [17] calculated $A(k, \omega)$ for the 1D Hubbard model in the thermodynamic strong coupling limit, and obtained

$$A(k,\omega) = (L-1) \left[ Z(Q_+(k,\omega)) + Z(Q_-(k,\omega)) \right] N(\omega), \tag{6.3}$$

where

$$Q_\pm(k,\omega) = k \pm \arccos(-\omega/2), \tag{6.4}$$

$$N(\omega) = \frac{1}{2\pi} \frac{1}{\sqrt{4-\omega^2}}, \tag{6.5}$$

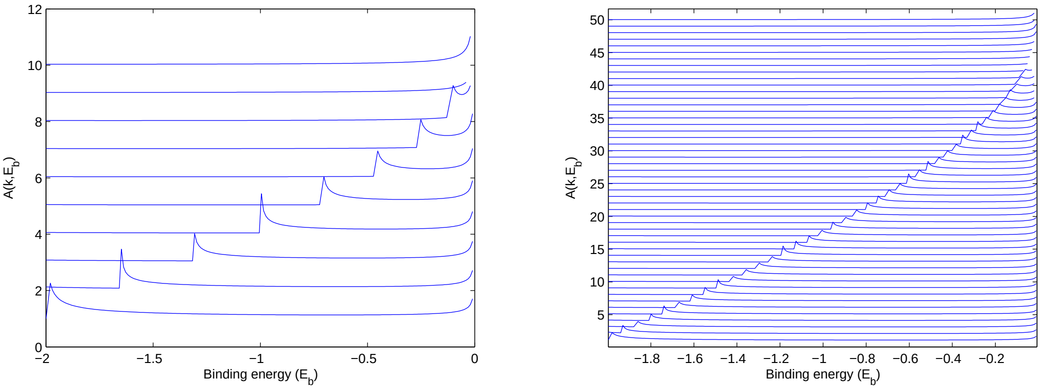

Figure 6.1: Plot of the spectral function $A(k,\omega)$ for the 1D Hubbard model, as a function of the binding energy $-2-\omega$, for several values of $k$: 10 values ranging from 0 to $\pi/2$ (left) and 50 values (right). More values of $k$ in the $[0,\pi]$ range represent a larger system. In order to avoid superposition of all the lines, a value proportional to $k$ was added to each line, thus maintaining the behavior of the lines.

---

and

$$(L-1)Z(Q) = \begin{cases} a + \frac{b}{\sqrt{\cos Q}} & \Leftarrow |Q| < \pi/2 \\ 0 & \Leftarrow |Q| \geq \pi/2 \end{cases} \tag{6.6}$$

where $a = -0.393$ and $b = 0.835$.

Figure 6.1 shows the plot of the spectral function using different amounts of values of $k$, from 0 to $\pi/2$. In 1D, the spectral function of any model has a double peak structure (see, for example, [18]). One of the peaks is determined by the spin velocity $E_b = kv_s$ and the other is determined by the charge velocity $v_q$. In the strong coupling limit, the spin velocity vanishes, since $v_s$ is proportional to $t^2/U$, thus explaining why one peak is always at $E_b = 0$.

Clearly, these graphics can be joined in a density plot on the $(k, E)$ plane, as shown in figure 6.2.

## 6.2 Helicoidal Hubbard model

As discussed in the previous chapters, the helicoidal Hubbard model with $t_\perp = 0$ is equivalent to the Hubbard chain. However, the momentum in the helicoidal Hubbard model keeps its "meaning" when transformed according to relation 2.12.

For the representation of the spectral function in the case of the helicoidal Hubbard model, we use expression 2.12, so that we can map the 2D twisted wave vector $(k_\parallel, k_\perp)$ into a 1D one and continue to use Parola's expression:

$$Q_\pm(k,\omega) \leftrightarrow Q_\pm(k_y/\Delta + k'_x, \omega) \tag{6.7}$$

The result is shown in Fig. 6.3. The intervals chosen are

$$\begin{array}{ccc} [0,0] & \rightarrow & [\pi,0] \\ [\pi,0] & \rightarrow & [\pi,\pi] \\ [\pi,\pi] & \rightarrow & [0,0] \end{array} \tag{6.8}$$

as written on the plot.

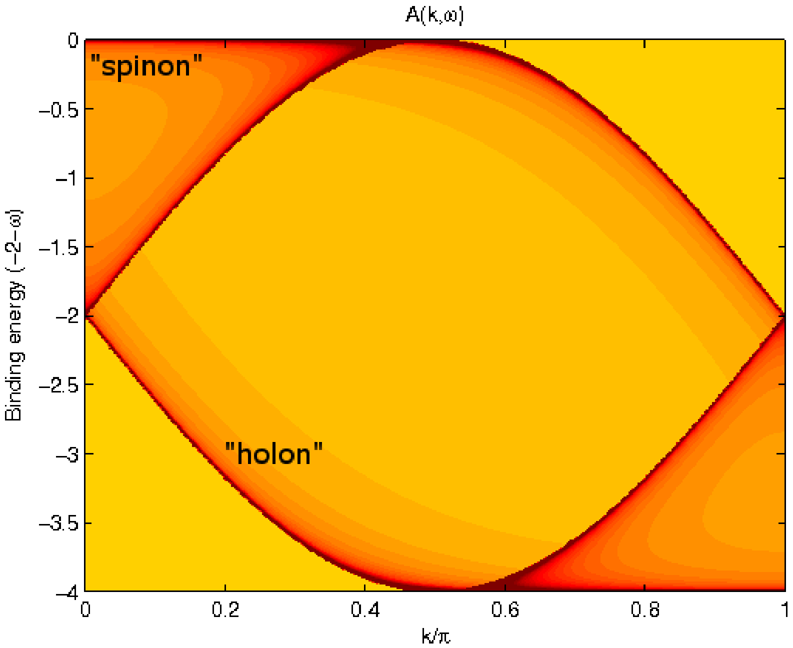

Figure 6.2: Density plot of the spectral function of the 1D Hubbard model, on the $(k, E)$ plane.

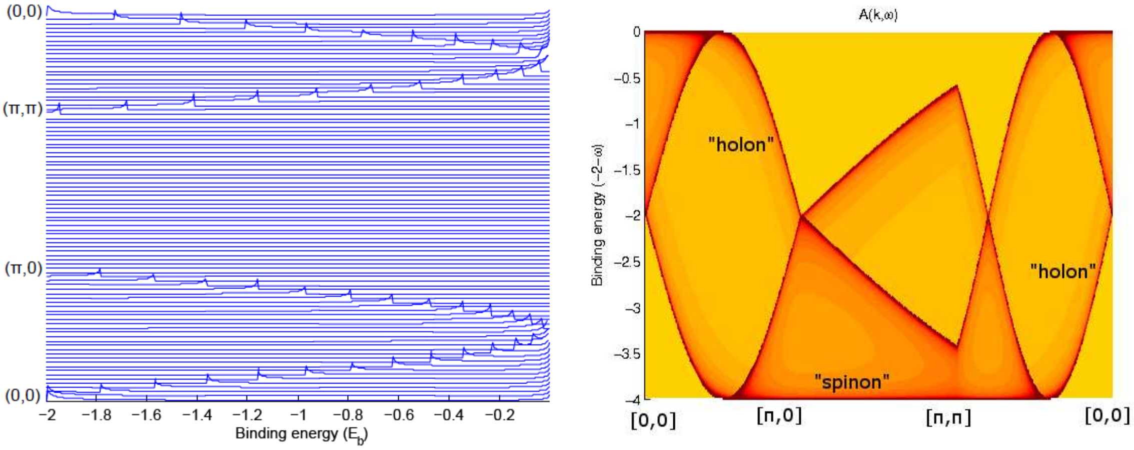

Figure 6.3: Spectral function for the helicoidal Hubbard model, as a function of the binding energy $-2 - \omega$, for several values of $\vec{k} = (k_{\parallel}, k_{\perp})$, as shown on the plot.

## Chapter 7

# Conclusions

The helicoidal Hubbard model was studied numerically and analytically in the $U \gg t_{\parallel} \gg t_{\perp} \gg t_{\parallel}^2/U$ limit.

A mean field approach allowed the numerical calculation of the magnetic phase diagram of the helicoidal Hubbard model. The phase diagrams of the 2D model and the helicoidal model with $t_{\parallel} = t_{\perp}$ are very similar. For instance, the antiferromagnetic phase is strictly confined to $n = 0$, and, at half filling, a transition from a paramagnetic phase to a ferromagnetic phase occurs at around $U = 12t$ in both models. The prediction of a spiral phase for low filling is in agreement with reference [13]. In order to achieve a better agreement between our results and those in the literature, future studies will include an increase of over an order of magnitude in the number of sites of the lattices used.

The thermodynamics of the tight-binding Hubbard model was also studied, using the exact diagonalization of the tight-binding 1D model with $N_h$ holes as a first approach to the strong-coupling helicoidal Hubbard model with $t_{\perp} = 0$. While the difficulty lied in the computation time required, for example, to count the number of states with each momentum, we were able to reduce that time by a factor of around 80 using a simpler method. Obtaining faster results meant we managed a more detailed study of the thermodynamic functions considered, whose results agreed with our expectations.

In order to study the $t_{\perp} \neq 0$ limit of the helicoidal Hubbard model, the quantum spin queue model was introduced. Our calculations led to the exact diagonalization of the strong-coupling helicoidal Hubbard model in the $U \gg t_{\parallel} \gg t_{\perp} \gg t_{\parallel}^2/U$ limit, whose results agreed with numerical ones. The particular case of one hole ($N_h = 1$) and one different spin was studied, due to the simplicity of the eigenvalues of the Hamiltonian for this case. Future work regarding these results may shed some light upon the study of the 2D Hubbard model and consequently, high temperature superconductivity.

Finally, we numerically calculated the spectral function of strong-coupling helicoidal Hubbard model using some results from its exact diagonalization when $t_{\perp} = 0$ and at half-filling, where the spin dynamics is determined by the Heisenberg Hamiltonian. Since spectral functions can be obtained from ARPES experiments, these calculations may be used to experimentally confirm the analytical results used.

# Appendix A

# Correlation functions for spinless fermions

In this section, a way to calculate correlation functions such as $\langle e^\dagger_{i+\Delta} e_i \rangle$ ($e^\dagger_i$ is the creation operator of a spinless fermion on site $i$) is presented. For application in this work, we shall treat the spinless fermions as holes. We begin by considering the usual definition of the wave number

$$k = \frac{2\pi}{L} n \qquad\qquad n = 0, \cdots, L-1. \tag{A.1}$$

Applying Fourier transforms to $\langle e^\dagger_{i+\Delta} e_i \rangle$ gives

$$\langle e^\dagger_{i+\Delta} e_i \rangle = \frac{1}{L} \sum_{k,k'} e^{i(kx_{i+\Delta} - k'x_i)} \langle e^\dagger_k e_{k'} \rangle = \frac{1}{L} \sum_k e^{ik\Delta} \langle e^\dagger_k e_k \rangle. \tag{A.2}$$

The summation can be calculated in terms of $n$,

$$\langle e^\dagger_{i+\Delta} e_i \rangle = \frac{1}{L} \sum_n e^{i\frac{2\pi\Delta}{L} n}. \tag{A.3}$$

If we assume the occupied states are the ones with lowest energy, with the relation dispersion in figure A.1, the non-vanishing terms are the ones that correspond to occupied states, that is, the occupied states are those with $n = n_1, n_1 + 1, \cdots, n_2$ and

$$\langle e^\dagger_{i+\Delta} e_i \rangle = \frac{1}{L} \sum_{n=n_1}^{n_2} e^{i\frac{2\pi\Delta}{L} n} = \frac{1}{L} e^{i\frac{\pi\Delta}{L}(n_1+n_2)} \frac{\sin \frac{\pi\Delta}{L} M}{\sin \frac{\pi\Delta}{L}}, \tag{A.4}$$

where $M = n_2 - n_1 + 1$ is the number of holes. For the dispersion relation in figure A.1, since we have $M$ states which are occupied with spinless fermions and those states are centered in terms of the values of $k$, we have

$$n_1 = \frac{L}{2} - \frac{M}{2} \qquad\qquad\qquad n_2 = \frac{L}{2} + \frac{M}{2}. \tag{A.5}$$

Replacing these in the previous result, and denoting the hole concentration by $m = M/L$,

$$\langle e^\dagger_{i+\Delta} e_i \rangle = \frac{1}{L} e^{i\pi\Delta} \frac{\sin(\pi\Delta m)}{\sin\left(\frac{\pi\Delta}{L}\right)}. \tag{A.6}$$

In the thermodynamic limit ($L \to \infty$), the expression simplifies to

$$\langle e^\dagger_{i+\Delta} e_i \rangle = e^{i\pi\Delta} \frac{\sin(\pi\Delta m)}{\pi\Delta}. \tag{A.7}$$

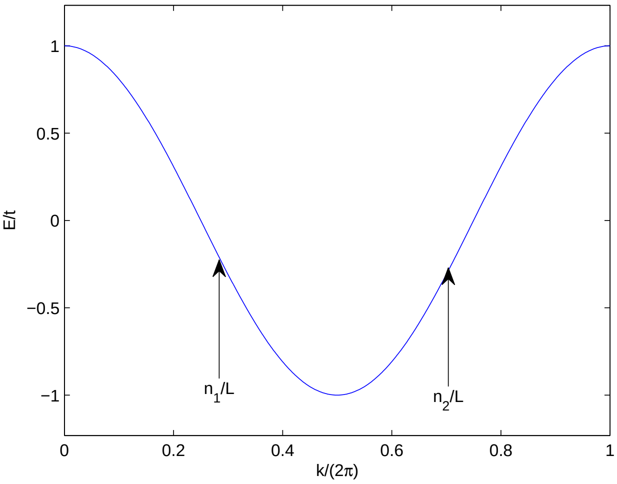

Figure A.1: Graphical representation of the relation dispersion for the 1D Hubbard model. The occupied states are the ones that correspond to values of $n$ between $n_1$ and $n_2$.

---

### Wick's theorem

Let us illustrate Wick's theorem by calculating a correlation function which requires its usage:

$$A = \langle (1 - e^\dagger_{i+1} e_{i+1})(1 - e^\dagger_i e_i)\rangle = 1 - \langle e^\dagger_{i+1} e_{i+1}\rangle - \langle e^\dagger_i e_i\rangle + \langle e^\dagger_{i+1} e_{i+1} e^\dagger_i e_i\rangle, \tag{A.8}$$

where $\langle e^\dagger_i e_i\rangle$ is the average number of holes per site $(m)$, which simplifies the above to

$$A = 1 - 2m + \langle e^\dagger_{i+1} e_{i+1} e^\dagger_i e_i\rangle. \tag{A.9}$$

The last term in this equation can be calculated using Wick's theorem, which states that

$$\langle e^\dagger_\alpha e_\beta e^\dagger_\gamma e_\delta\rangle = \langle e^\dagger_\alpha e_\beta\rangle\langle e^\dagger_\gamma e_\delta\rangle + \langle e^\dagger_\alpha e_\gamma\rangle\langle e_\beta e^\dagger_\gamma\rangle. \tag{A.10}$$

In our case, Wick's theorem transforms A.9 into

$$A = 1 - 2m + \langle e^\dagger_{i+1} e_{i+1}\rangle\langle e^\dagger_i e_i\rangle - \langle e^\dagger_{i+1} e_i\rangle\langle e^\dagger_i e_{i+1}\rangle, \tag{A.11}$$

which, denoting the concentration of particles by $n = 1 - m$, finally becomes

$$\langle (1 - e^\dagger_{i+1} e_{i+1})(1 - e^\dagger_i e_i)\rangle = n^2 - \frac{\sin^2(\pi m)}{\pi^2} \tag{A.12}$$

# Appendix B

# The Möbius inversion formula

The Möbius function $\mu(d)$ can only take 3 distinct values:

$$\begin{array}{ll} \mu(d) = 1 & \Leftarrow d = 1 \\ \mu(d) = (-1)^k & \Leftarrow d \text{ is the product of } k \text{ distinct prime numbers} \\ \mu(d) = 0 & \Leftarrow d \text{ is divisible by a square number greater than 1} \end{array} \tag{B.1}$$

This function is used in the *Möbius inversion formula*, which is the following proposition:

Let $f(n)$ and $g(n)$ be functions or a natural number $n$. Then,

$$f(n) = \sum_{d|n} g(d), \tag{B.2}$$

where $d|n$ denotes "$d$ divides $n$", if and only if

$$g(n) = \sum_{d|n} \mu(d) f(n/d). \tag{B.3}$$

Likewise, for functions $f$ and $g$ of $m$ natural numbers $n_1, \cdots, n_m$, it can be shown that

$$f(n_1, \cdots, n_m) = \sum_{d|n_1,\cdots,n_m} g(n_1/d, \cdots, n_m/d) \tag{B.4}$$

is equivalent to

$$g(n_1, \cdots, n_m) = \sum_{d|n_1,\cdots,n_m} \mu(d) f(n_1/d, \cdots, n_m/d). \tag{B.5}$$

# Bibliography

[1] V. Celebonovic, "The Hubbard model: basic notions and selected applications", Journal of Optoelectronics and Advanced Materials, 11, 2009.

[2] M. Dressel, "Spin-charge separation in quasi one-dimensional organic conductors", Nature (2003) 90:337-344.

[3] H. Bethe, "Zur Theorie der Metalle" ["The theory of metals"], Z. Phys. A 71, 1931.

[4] E. H. Lieb, "The Hubbard model: some rigorous results and open problems", arXiv:cond-mat/9311033.

[5] F. H. L. Essler, H. Frahm, F. Gohmann, A. Klumper and V. Korepin, "The One-Dimensional Hubbard Model", Cambridge Press, 2005.

[6] A. B. Harris, R. V. Lange, "Single-Particle Excitations in Narrow Energy Bands", Phys. Rev. 157, 1967

[7] R. G. Dias and J. M. B. Lopes dos Santos, "Simple representation of the eigenstates of the $U \to \infty$ one dimensional Hubbard model", J. Phys. I France 2 (1992) 1889-1897.

[8] Shi-Jie Xiong, "Bethe ansatz study of 1+1 dimensional Hubbard model", Z. Phys. B 89, 1992.

[9] W. Wang and Shi-jie Xiong, "Possible first order phase transition in the one-dimensional helical Hubbard model", Phys. Lett. A 156, 1991.

[10] R.T. Scalettar, "Elementary Introduction to the Hubbard Model", lecture notes, UC Davis, http://leopard.physics.ucdavis.edu/rts/p210/hubbard7.pdf.

[11] M. Dzierzawa, "Hartree-Fock theory of spiral magnetic order in the 2-d Hubbard model", Z. Phys. B 86, 1992.

[12] A. Singh, Z. Tesanovic and J. H. Kim, "Instability of the spiral state of the doped Hubbard model", Pramana Journal of Physics, Vol. 38, 1992.

[13] S. Sarker et al., "Spiral states in the square-lattice Hubbard model", Phys. Review B 43, 1991.

[14] A. Mielke, "The One-Dimensional Hubbard Model for Large or Infinite $U$", Journal of Statistical Physics, Vol. 62, 1991.

[15] M. Ogata and H. Shiba, "Bethe-ansatz wave function, momentum distribution, and spin correlation in the one-dimensional strongly correlated Hubbard model", Phys. Rev. B 41, 1990.

[16] C. Kim et al., "Complex Materials Research by Angle-Resolved Photoemission Spectroscopy: Challenging the Mystery of the High $T_c$ Superconductivity", SSRL Highlights Archive, July 2001.

[17] A. Parola and S. Sorella, "Spin-charge decoupling and the Green's function of the one-dimensional Mott insulators", Phys. Review B 45, 1992.

[18] V. Lante and A. Parola, "Spin-charge decoupling and the photoemission line-shape in one-dimensional insulators", Phys. Rev. B 80, 2009.